Mon. Not. R. Astron. Soc. **000**, 1–23 () Printed 1 April 2011 (MN LATEX style file v2.2)

Spectral and algebraic instabilities in thin Keplerian discs under poloidal and toroidal magnetic fields

Yuri M. Shtemler[1⋆], Michael Mond[1], and Edward Liverts[1]
[1] *Department of Mechanical Engineering, Ben-Gurion University of the Negev, P.O. Box 653, Beer-Sheva 84105, Israel*

Accepted —. Received —-; in original form —-

ABSTRACT

Linear instability of two equilibrium configurations with either poloidal (I) or toroidal (II) dominant magnetic field components are studied in thin vertically-isothermal Keplerian discs. Solutions of the stability problem are found explicitly by asymptotic expansions in the small aspect ratio of the disc. In both equilibrium configurations the perturbations are decoupled into in-plane and vertical modes. For equilibria of type I those two modes are the Alfvén-Coriolis and sound waves, while for equilibria of type II they are the inertia-Coriolis and magnetosonic waves. Exact expressions for the growth rates as well as the number of unstable modes for type I equilibria are derived. Those are the discrete counterpart of the continuous infinite homogeneous cylinder magnetorotational (MRI) spectrum. It is further shown that the axisymmetric MRI is completely suppressed by dominant toroidal magnetic fields (i.e. equilibria of type II). This renders the system prone to either non-axisymmetric MRI or non-modal algebraic growth mechanisms. The algebraic growth mechanism investigated in the present study occurs exclusively due to the rotation shear, generates the inertia-Coriolis driven magnetosonic modes due to non-resonant or resonant coupling that induces, respectively, linear or quadratic temporal growth of the perturbations.

Key words: accretion, accretion discs - MHD-instabilities

1 INTRODUCTION

The stability properties of Keplerian disks have been a focus of intensive investigation of theoretical astrophysicists over the last decades, pertaining to the problem of angular momentum transfer in accretion disks. Traditionally, two routes have been taken by researchers in order to elucidate various aspects of that topic. Thus, the results of the analytical study of magneto-rotational instability (MRI) in an infinitely long cylinder [Velichov (1959); Chandrasechar (1960)] have been adopted for the thin disks in order to derive criteria for the spectral stability under various conditions [Balbus & Hawley (1991)]. On the second route, numerical calculations have been performed, usually by employing the shearing-box model, in order to study the nonlinear evolution of small perturbations, and their subsequent development into full sustainable turbulence [Brandenburg et al. (1995); Hawley et al. (1996); Bodo et al. (2008); Regev & Umurhan (2008)]. The main thrust of both routes has been to establish the MRI as the main generator of sustainable turbulence. Notwithstanding accumulating analytical as well as numerical results, the notion of the MRI as a driver of turbulence and angular momentum transport has recently been shown to suffer from non-trivial difficulties in the sheer use of the shearing box in the simulations [Bodo et al. (2008); Regev & Umurhan (2008)] as well as in doubts regarding the numerical convergence and resolution [Lesur & Longaretti (2007); Fromang & Papaloizou (2007); Fromang et al. (2007); Pessah et al. (2007)]. In addition, it has recently been shown that if the thin disk geometry is taken into account both the growth rates as well as the number of unstable MRI modes are greatly reduced and are decreasing functions of the disk thickness [Coppi & Keyes (2003); Liverts & Mond (2009)]. In parallel, an alternative route that has recently emerged within which the dynamical response of the thin disks is investigated asymptotically in the small thickness-to-radius ratio has been shown to lead to fruitful and physically sound results. In particular, applying such strategy it has been shown that algebraic non-modal instabilities are the primary source of pure hydrodynamical activity [Umurhan et al.

⋆ E-mail: shtemler@bgu.ac.il; mond@bgu.ac.il; eliverts@bgu.ac.il

(2006); Rebusco et al. (2009); Shtemler et al. (2010)]. Furthermore, the mechanism for such non-exponential growth has been identified as the resonant as well as non-resonant interaction between inertia-Coriolis modes and sound waves [Shtemler et al. (2010)]. Interestingly enough, such an investigation has never been carried out for magnetized disks that are described by the magnetohydrodynamic (MHD) model. It is thus one of the main goals of the current work to carry out a comprehensive study of the MHD response of thin Keplerian disks taking into account their true thin-disk geometry.

In that connection note that although the magnetic field configuration in real discs is largely unknown, in the initial stage of the disc rotation the poloidal field is commonly accepted as the dominant component. However, observations and numerical simulations indicate that toroidal magnetic field may be of the same order of magnitude, or even dominate the poloidal magnetic field [see e.g. Terquem & Papaloizou (1996); Papaloizou & Terquem (1997); Hawley & Krolik (2002); Proga (2003)]. In particular, the unstable modes give rise to MRI [Balbus & Hawley (1991)] which amplifies considerably the toroidal component of the magnetic field to the point that it may dominate the original axial field [Pessah & Psaltis (2005); Begelman & Pringle (2007)]. It is of great importance therefore to investigate how the magnetic field topology influences the stability properties of the disc. The way to do that is to follow the linear problem in terms of a toroidal dominated magnetic field instead of poloidal one leading to MRI. Thus, one more goal of the present work is investigation of two types of magnetic field equilibrium configurations with either poloidal or toroidal dominated magnetic field component and their relations with spectral and non-modal mechanisms of instability in thin discs.

The paper is organized as follows. The dimensionless governing equations and their approximation to leading order in small aspect ratio of the steady-state disc are presented in the next Section. Two magnetic field configurations with dominated axial (I) and dominated toroidal (II) equilibrium magnetic fields are also described in that Section. Sections 3 and 4 describe the principal hydro-magnetic modes which can propagate in thin Keplerian discs for I and II types of equilibria, respectively. Summary and discussion are presented in Section 5. In Appendix A the general relations for comparable in-plane components of the equilibrium magnetic field are discussed in the limit of large plasma beta, and the qualitative stability analysis is made.

2 THE PHYSICAL MODEL FOR THIN KEPLERIAN DISCS

The stability of radially as well as axially stratified rotating plasma in thin vertically isothermal discs threaded by a magnetic field is considered. Viscosity, electrical resistivity, and radiation effects are ignored.

2.1 Governing equations

As a first step, all physical variables are transformed to non-dimensional quantities by using the following characteristic values [Shtemler et al. (2009); Shtemler et al. (2010)]:

$$t_*=\frac{1}{\Omega_*},\ V_*=\frac{r_*}{t_*},\ L_*=V_*t_*,\ m_*=m_i,\ n_*=n_i,$$

$$\Phi_*={V_*}^2,\ c_{S*}=\sqrt{T_*/m_*},\ \ P_*=m_*n_*c_{S*}^2,\ j_*=\frac{c}{4\pi}\frac{B_*}{r_*},\ E_*=\frac{V_*B_*}{c}. \tag{1}$$

Here $\Omega_*=(GM_c/r_*^3)^{1/2}$ is the Keplerian angular velocity of the fluid at the characteristic radius r_* that belongs to the Keplerian portion of the disc; G is the gravitational constant; M_c is the total mass of the central object; c is the speed of light; Φ_* is the characteristic value of the gravitational potential; the characteristic mass and number density equal to the ion mass and number density, $m_*=m_i$ and $n_*=n_i$. The characteristic values of the electric current density and electric field, j_* and E_* have been chosen consistently with Maxwell's equations; c_{S*} is the characteristic sound velocity; $T_*=T(r_*)$ is the characteristic temperature; the characteristic magnetic field is specified below depending on the magnetic field configuration: $B_*=B_z(r_*)$ if the axial equilibrium magnetic field dominates or of the order toroidal one, and $B_*=B_\theta(r_*)$ otherwise; the dimensional equilibrium temperature and the two components of the equilibrium magnetic field, $T(r)$ and $B_z(r)$, $B_\theta(r)$, respectively, are free functions.

The resulting dimensionless dynamical equations for vertically isothermal discs are:

$$\frac{D\mathbf{V}}{Dt}=-\frac{1}{M_S^2}\frac{\nabla P}{n}-\nabla\Phi+\frac{1}{\beta M_S^2}\frac{\mathbf{j}\times\mathbf{B}}{n}, \tag{2}$$

$$\frac{\partial n}{\partial t}+\nabla\cdot(n\mathbf{V})=0, \tag{3}$$

$$\frac{\partial\mathbf{B}}{\partial t}+\nabla\times\mathbf{E}=0,\ \nabla\cdot\mathbf{B}=0, \tag{4}$$

$$\mathbf{E}=-\mathbf{V}\times\mathbf{B}, \tag{5}$$

$$P=nT. \tag{6}$$

Here $\nabla P = \bar{c}_S^2 \nabla n$ for vertically isothermal discs, and the dimensionless equilibrium sound speed is given by $\bar{c}_S^2 = \partial P/\partial n \equiv T(r)$. Standard cylindrical coordinates $\{r, \theta, z\}$ are adopted throughout the paper with the associated unit vectors $\{\mathbf{i_r}, \mathbf{i}_\theta, \mathbf{i_z}\}$; $\mathbf{V}$ is the plasma velocity; t is time; $D/Dt = \partial/\partial t + (\mathbf{V}\cdot\nabla)$ is the material derivative; $\Phi(r,z) = -(r^2+z^2)^{-1/2}$ is the gravitational potential due to the central object; $\mathbf{B}$ is the magnetic field, $\mathbf{j} = \nabla \times \mathbf{B}$ is the current density; $\mathbf{E}$ is the electric field; $P = P_e + P_i$ is the total plasma pressure; $P_l = n_l T_l$ are the partial species pressures ($l = e, i$); $T = T_e = T_i$ is the plasma temperature; subscripts e and i denote electrons and ions, respectively. Note that a preferred direction is tacitly defined here, namely, the positive direction of the z axis is chosen according to positive Keplerian rotation. The dimensionless coefficients M_S and β are the Mach number and the characteristic plasma beta, respectively:

$$M_S = \frac{V_*}{c_{S*}},\ \beta = \frac{P_*}{B_*^2}. \tag{7}$$

Zero conditions at infinity for the in-plane magnetic field are adopted, namely:

$$B_r = 0,\ \ B_\theta = 0 \quad \text{for}\ \ z = \pm\infty. \tag{8}$$

The boundary condition for the axial velocity will be specified below as the least possible divergence at infinity. As will be seen later on, despite such unbounded growth the axial mass flux tends to zero far away from the mid-plane due to the fast vanishing of number density at $z = \pm\infty$. To simplify the further treatment of Maxwell's equations, both the hydro-magnetic basic configuration and perturbations are assumed to be axisymmetric.

A common property of thin Keplerian discs is their highly compressible motion with large Mach numbers [Frank et al. (2002)]. Furthermore, the characteristic effective semi-thickness of the equilibrium disc $H_* = H(r_*)$ ($H = H(r)$ is the local semi-thickness) is defined so that the disc aspect ratio ϵ equals the inverse Mach number:

$$\frac{1}{M_S} = \epsilon = \frac{H_*}{r_*} \ll 1. \tag{9}$$

Thus, the thin disc approximation means

$$\frac{1}{M_S} = \sqrt{\frac{r_* T_*}{G M_c}} = \epsilon \ll 1, \tag{10}$$

where

$$M_S = \frac{V_*}{c_{S*}},\ \ V_* = r_*\Omega_*,\ \Omega_* = \sqrt{\frac{GM_c}{r_*^3}},\ \ c_{S*} = \sqrt{T_*},\ \ H_* = \frac{c_{S*}}{\Omega_*}\,.$$

The smallness of ϵ means that dimensionless axial coordinate is also small, i.e. $z/r_* \sim \epsilon$ ($|z| \lesssim H_*$), and consequently the following rescaled quantities may be introduced in order to further apply the asymptotic expansions in ϵ [similar to Shtemler et al. (2009); Shtemler et al. (2010)]:

$$\zeta = \frac{z}{\epsilon} \sim \epsilon^0,\ \ \bar{H}(r) = \frac{H(r)}{\epsilon} \sim \epsilon^0, \tag{11}$$

where $\bar{H}(r) = \bar{c}_S(r)/\bar{\Omega}(r)$ is the scaled semi-thickness of the disc.

2.2 Equilibrium configurations

We start by deriving the steady state solution. It is first noted that the asymptotic expansion for the time-independent gravitational potential is given by:

$$\Phi(r,\zeta) = \bar{\Phi}(r) + \epsilon^2\bar{\phi}(r,\zeta),\ \ \bar{\Phi}(r) = -\frac{1}{r},\ \ \bar{\phi}(r,\zeta) = \frac{1}{2}\zeta^2\bar{\Omega}^2(r) + O(\epsilon^2),\ \ r > 1 >> \epsilon. \tag{12}$$

Substituting (12) into Eqs. (2)-(6) and setting the partial derivatives with respect to time to zero yield to leading order in ϵ

$$\frac{\bar{V}_\theta^2}{r} = \frac{d\bar{\Phi}(r)}{dr},\ \ \frac{\bar{c}_S^2(r)}{\bar{n}}\frac{\partial\bar{n}}{\partial\zeta} = -\frac{\partial\bar{\phi}(r,\zeta)}{\partial\zeta}. \tag{13}$$

Thus, the velocity as well as the number density are as follows:

$$V_r = o(\epsilon^2),\ \ V_\theta = \epsilon^0\bar{V}_\theta(r) + O(\epsilon^2),\ \ V_z = o(\epsilon^2),\ \ n \cong \epsilon^0\bar{n} \equiv \epsilon^0\bar{N}(r)\bar{\nu}(\eta), \tag{14}$$

where $o(\epsilon) \ll \epsilon$, $O(\epsilon) \sim \epsilon$, and

$$\bar{V}_\theta(r) = r\bar{\Omega}(r),\ \ \bar{\Omega}(r) = r^{-3/2},\ \ \bar{\nu}(\eta) = \exp(-\eta^2/2),\quad \eta = \zeta/\bar{H}(r). \tag{15}$$

Two quite different equilibrium magnetic configurations will be considered below, namely one with comparable magnitudes of the axial and toroidal components of the magnetic field (mainly studied for the dominant poloidal magnetic field, while the general case of comparable components of the magnetic field is discussed in Appendix A), and the other with dominant toroidal component. The two equilibria (denoted I and II below) are distinguished by different scaling of the physical variables

Table 1. Scales in ϵ of the equilibrium variables for two types of equilibria (I) and (II).

$f=\epsilon^{\bar{S}}\bar{f}$	n	V_r	V_θ	V_z	B_r	B_θ	B_z	j_r	j_θ	j_z
I, $\bar{S}$	0	>2	0	>2	>2	0	0	>2	0	0
II, $\bar{S}$	0	>2	0	>2	>2	0	1	>2	1	0

with ϵ which generally may be written as $f(r,\zeta)=\epsilon^{\bar{S}}\bar{f}(r,\zeta)$. All equilibrium variables are written in the leading order in ϵ, and depend on the radial variable only. The exceptions are the number density and the pressure that depend on the axial coordinate in a self-similar manner with radius-dependent amplitude. The toroidal and axial magnetic fields as well as the disc thickness and the amplitude factor, $\bar{N}(r)$, in the number density are arbitrary functions of the radial variable. Those functions specify the equilibrium state.

To start the equilibrium description it is first assumed that both types of equilibria under the current study are characterized by a toroidal component of the magnetic field that is of order ϵ^0. In contrast, in one equilibrium system (I) the axial component of the magnetic field is of order ϵ^0 as well, while in the other system (II) it is of order ϵ. These assumptions together with relations (12)-(15), determine the order in ϵ of the rest of the physical variables:

(I) Comparable equilibrium magnetic field components

$$B_r=o(\epsilon^2),\ \ B_\theta\cong\epsilon^0\bar{B}_\theta(r),\ \ B_z\cong\epsilon^0\bar{B}_z(r),j_r=o(\epsilon^2),\ \ j_\theta\cong\epsilon^0\bar{j}_\theta(r)\equiv-\epsilon^0\frac{d\bar{B}_z}{dr},\ \ j_z\cong\epsilon^0\bar{j}_z\equiv\epsilon^0\frac{1}{r}\frac{d(r\bar{B}_\theta)}{dr}. \tag{16}$$

(II) Dominant equilibrium toroidal magnetic field

$$B_r=o(\epsilon^2),\ \ B_\theta\cong\epsilon^0\bar{B}_\theta(r),\ \ B_z\cong\epsilon\bar{B}_z(r),j_r=o(\epsilon^2),\ \ j_\theta\cong\epsilon\bar{j}_\theta(r)\equiv-\epsilon\frac{d\bar{B}_z}{dr},\ \ j_z\cong\epsilon^0\bar{j}_z\equiv\epsilon^0\frac{1}{r}\frac{d(r\bar{B}_\theta)}{dr}. \tag{17}$$

For convenience the results are summarized in Table 1. It is noted finally that to lowest order in ϵ the magnetic field configurations under consideration do not influence the steady-state properties of the disk. As will be seen in the following sections, this situation changes dramatically when small perturbations are considered.

2.3 Perturbed thin discs

In general for the unsteady nonlinear case the dependent variables are scaled in ϵ in the following way:

$$f(r,\zeta,t)=\epsilon^{\bar{S}}\bar{f}(r,\zeta)+\epsilon^{S'}f'(r,\zeta,t). \tag{18}$$

Here $f(r,\zeta,t)$ stands for any dependent variable, the bar and the prime denote equilibrium and perturbed variables; each perturbed variable is characterized by some power S' that is different for two types of equilibria I and II. The various cases are summarized in (Table 2).

3 DYNAMICAL EQUATIONS FOR THE PERTURBED DISC: TYPE I EQUILIBRIA

Consider the general dynamic equations for the perturbed disc equilibria of type I, namely thin discs under the effect of a magnetic field with comparable poloidal and toroidal components. Then the detailed stability study is carried out for zero toroidal magnetic field, while a qualitative analysis of the comparable poloidal and toroidal components is presented in Appendix A.

3.1 The reduced nonlinear equations

Substituting (12)-(18) into (2) - (6) yields to leading order in ϵ the following system of the reduced non-linear equations that governs the dynamical behavior of thin discs:

$$\frac{\partial V_r'}{\partial t}-2\bar{\Omega}(r)V_\theta'+V_z'\frac{\partial V_r'}{\partial\zeta}-\frac{1}{\beta}\frac{\bar{B}_z(r)}{\bar{n}+n'}\frac{\partial B_r'}{\partial\zeta}=0, \tag{19}$$

$$\frac{\partial V_\theta'}{\partial t}+\frac{1}{r}\frac{d(r^2\bar{\Omega})}{dr}V_r'+V_z'\frac{\partial V_\theta'}{\partial\zeta}-\frac{1}{\beta}\frac{\bar{B}_z(r)}{\bar{n}+n'}\frac{\partial B_\theta'}{\partial\zeta}=0, \tag{20}$$

$$\frac{\partial V_z'}{\partial t}+\bar{c}_S^2(r)\frac{\bar{n}}{\bar{n}+n'}\frac{\partial}{\partial\zeta}(\frac{n'}{\bar{n}})+\frac{1}{\beta}\bar{B}_\theta(r)\frac{\partial}{\partial\zeta}(\frac{B_\theta'}{\bar{n}+n'})=-\frac{1}{2}\frac{\partial}{\partial\zeta}(V_z'^2+\frac{1}{\beta}\frac{B_\theta'^2+B_r'^2}{\bar{n}+n'}), \tag{21}$$

$$\frac{\partial n'}{\partial t}+\frac{\partial[(\bar{n}+n')V_z']}{\partial\zeta}=0, \tag{22}$$

Table 2. Scales in ϵ of the perturbed variables for two types of equilibria (I) and (II).

$f = \epsilon^{\bar{S}} \bar{f} + \epsilon^{S'} f'$	n	V_r	V_θ	V_z	B_r	B_θ	B_z	j_r	j_θ	j_z
I, S'	0	1	1	1	0	0	1	-1	-1	0
II, S'	0	0	0	1	0	0	1	-1	-1	0

$$\frac{\partial B_r'}{\partial t} - \bar{B}_z(r)\frac{\partial V_r'}{\partial \zeta} = -\frac{\partial V_z' B_r'}{\partial \zeta}, \tag{23}$$

$$\frac{\partial B_\theta'}{\partial t} - \bar{B}_z(r)\frac{\partial V_\theta'}{\partial \zeta} - r\frac{d\bar{\Omega}}{dr}B_r' = -\frac{\partial V_z' B_\theta'}{\partial \zeta} - \bar{B}_\theta(r)\frac{\partial V_z'}{\partial \zeta}. \tag{24}$$

The system of equations (19) - (24) is subject to the boundary condition of least possible divergence for the axial velocity at infinity along with the conditions for the in-plane magnetic field as follows from (8)

$$B_r' = 0, \;\; B_\theta' = 0 \quad \text{for} \quad \zeta = \pm\infty. \tag{25}$$

Both poloidal and toroidal components of the perturbed magnetic field, B_r' and B_z' , are expressed through the magnetic flux function, Ψ', which provides the divergent free magnetic field, $\nabla\cdot\mathbf{B} = 0$. Here the equation for B_r' is obtained by differentiating by ζ the equation for Ψ', while the corresponding equation for the perturbed axial magnetic field, B_z', decouples from the rest equations, and drops out from the governing system of equations (19) - (24). Equation (21) has been derived with the help of the second steady-state relation (14). Furthermore, the radial derivatives drop out from the system of Eqs. (19) - (25). This, it should be stressed, is so not due to a frozen coefficients assumption, but is a direct result of the thin disc geometry. An important conclusion from the absence of radial derivatives in the reduced system of equations of the thin disc approximation is that transient non-exponential growth is not possible in such configuration. As will subsequently be shown (see Section 4 of the present paper), this picture changes dramatically when the dominant magnetic fields are toroidal, in which case the only possible axisymmetric instability is due to non-modal algebraic transient growth.

As the radial coordinate is a mere parameter in the set of the reduced equations, it is convenient to replace the physical variables by the following self-similar quantities:

$$\tau = t, \quad \eta = \frac{\zeta}{\bar{H}(r)}, \tag{26}$$

such that the derivatives in the new and old variables are related as follows:

$$\frac{\partial}{\partial t} = \frac{\partial}{\partial \tau}, \;\; \frac{\partial}{\partial \zeta} = \frac{1}{\bar{H}(r)}\frac{\partial}{\partial \eta}. \tag{27}$$

Finally, system (19) - (25) may be written in a simpler form by introducing the following scaled dependent variables:

$$\mathbf{v}(\tau, r, \eta) = \frac{\mathbf{V}'}{\bar{c}_S(r)}, \;\; \nu(\tau, r, \eta) = \frac{n'}{\bar{N}(r)}, \;\; \mathbf{b}(\tau, r, \eta) = \frac{\mathbf{B}'}{\bar{B}_z(r)}. \tag{28}$$

Below for convenience and with no confusion the notation t for the time variable is reinstated instead of the new variable τ. This yields the following system of equations that depend parametrically on the radius:

$$\frac{1}{\bar{\Omega}(r)}\frac{\partial v_r}{\partial t} - 2v_\theta - \frac{1}{\bar{\beta}_z(r)}\frac{1}{\bar{\nu}(\eta)+\nu}\frac{\partial b_r}{\partial \eta} = -v_z\frac{\partial v_r}{\partial \eta}, \tag{29}$$

$$\frac{1}{\bar{\Omega}(r)}\frac{\partial v_\theta}{\partial t} + \frac{1}{2}v_r - \frac{1}{\bar{\beta}_z(r)}\frac{1}{\bar{\nu}(\eta)+\nu}\frac{\partial b_\theta}{\partial \eta} = -v_z\frac{\partial v_\theta}{\partial \eta}, \tag{30}$$

$$\frac{1}{\bar{\Omega}(r)}\frac{\partial v_z}{\partial t} + \frac{\bar{\nu}(\eta)}{\bar{\nu}(\eta)+\nu}\frac{\partial}{\partial \eta}\left(\frac{\nu}{\bar{\nu}(\eta)}\right) + \frac{\bar{S}(r)}{\bar{\beta}_z(r)}\frac{\partial}{\partial \eta}\left[\frac{b_\theta}{\bar{\nu}(\eta)+\nu}\right] = -\frac{1}{2}\frac{\partial}{\partial \eta}\left[v_z^2 + \frac{1}{\bar{\beta}_z(r)}\frac{b_\theta^2 + b_r^2}{\bar{\nu}(\eta)+\nu}\right], \tag{31}$$

$$\frac{1}{\bar{\Omega}(r)}\frac{\partial \nu}{\partial t} + \frac{\partial[(\bar{\nu}(\eta)+\nu]v_z}{\partial \eta} = 0, \tag{32}$$

$$\frac{1}{\bar{\Omega}(r)}\frac{\partial b_r}{\partial t} - \frac{\partial v_r}{\partial \eta} = -\frac{\partial(v_z b_r)}{\partial \eta}, \tag{33}$$

$$\frac{1}{\bar{\Omega}(r)}\frac{\partial b_\theta}{\partial t} - \frac{\partial v_\theta}{\partial \eta} + \frac{3}{2}b_r = -\frac{\partial(v_z b_\theta)}{\partial \eta} - \bar{S}(r)\frac{\partial v_z}{\partial \eta}, \tag{34}$$

supplemented by the boundary condition of least possible divergence for the axial velocity along with the vanishing conditions for the in-plane magnetic field at infinity. Here the Keplerian epicyclical frequency, $\bar{\chi}(r) = \bar{\Omega}(r)$ has been employed; $\bar{\nu}(\eta)$ is the scaled equilibrium density; $\bar{\beta}_z(r)$ and $\bar{\beta}_\theta(r)$ are the local axial and toroidal plasma beta functions:

$$\bar{\beta}_z(r)=\beta\frac{\bar{N}(r)\bar{c}_S^2(r)}{\bar{B}_z^2(r)},\quad \bar{\beta}_\theta(r)=\beta\frac{\bar{N}(r)\bar{c}_S^2(r)}{\bar{B}_\theta^2(r)},\quad \bar{S(r)}=\sqrt{\frac{\bar{\beta}_z(r)}{\bar{\beta}_\theta(r)}}\equiv\frac{\bar{B}_\theta(r)}{\bar{B}_z(r)},\tag{35}$$

where both local parameters $\bar{\beta}_z(r)$ and $\bar{\beta}_\theta(r)$ are proportional to the characteristic plasma beta, β.

Relations (29)-(35) form the full nonlinear MHD problem in the thin disc approximation and are named as defined above, the reduced nonlinear equations.

3.2 The linear problem.

Assuming now that the perturbations are small, the system of equations (29)-(34) may be linearized about the steady-state equilibrium solution. This yields:

$$\frac{1}{\bar{\Omega}(r)}\frac{\partial v_r}{\partial t}-2v_\theta-\frac{1}{\bar{\beta}_z(r)\bar{\nu}(\eta)}\frac{\partial b_r}{\partial\eta}=0,\tag{36}$$

$$\frac{1}{\bar{\Omega}(r)}\frac{\partial v_\theta}{\partial t}+\frac{1}{2}v_r-\frac{1}{\bar{\beta}_z(r)\bar{\nu}(\eta)}\frac{\partial b_\theta}{\partial\eta}=0,\tag{37}$$

$$\frac{1}{\bar{\Omega}(r)}\frac{\partial b_r}{\partial t}-\frac{\partial v_r}{\partial\eta}=0,\tag{38}$$

$$\frac{1}{\bar{\Omega}(r)}\frac{\partial b_\theta}{\partial t}-\frac{\partial v_\theta}{\partial\eta}+\frac{3}{2}b_r=-\bar{S}(r)\frac{\partial v_z}{\partial\eta},\tag{39}$$

$$\frac{1}{\bar{\Omega}(r)}\frac{\partial v_z}{\partial t}+\frac{\partial}{\partial\eta}(\frac{\nu}{\bar{\nu}(\eta)})=-\frac{\bar{S}(r)}{\bar{\beta}_z(r)}\frac{\partial}{\partial\eta}[\frac{b_\theta}{\bar{\nu}(\eta)}],\tag{40}$$

$$\frac{1}{\bar{\Omega}(r)}\frac{\partial\nu}{\partial t}+\frac{\partial[\bar{\nu}(\eta)v_z]}{\partial\eta}=0.\tag{41}$$

For definiteness the characteristic magnetic field is specified as the dimensional axial component of the equilibrium magnetic field $B_*=B_z(r_*)$.

The general case of comparable poloidal and toroidal components of the equilibrium magnetic field is presented in Appendix A for perturbations of type I. A qualitative analysis is done of the influence of the equilibrium toroidal magnetic field on the disc stability in the limit of large plasma beta. In the case of small plasma beta ($\beta\lesssim 1$) two principal modes, namely the Alfvén-Coriolis (AC) and the magnetosonic (MS) modes, are strongly coupled, while in the limit of large plasma beta, AC mode decouples on its characteristic scale from the MS mode. This leaves the resulting dispersion relation the same as in the case of zero toroidal magnetic field, and the influence of the toroidal magnetic field is reduced to excitation of the AC-driven MS mode. On the characteristic scale of MS's mode, a stable MS mode decouples from the AC mode and the influence of the equilibrium toroidal magnetic field is reduced to excitation of the stable MS-driven AC mode.

To simplify the analysis, the equilibrium toroidal magnetic field is set to zero for type I equilibria, or equivalently, $\bar{\beta}_\theta(r)=\infty$. Under such conditions the reduced linearized system (36) - (41) is divided into two decoupled sub-systems that describe the dynamics of two different modes, namely: the Alfvén-Coriolis and the sound modes. It is indeed the approximation that is adopted in the remaining of the current analysis of type I equilibria.

3.3 Linear stability analysis for the Alfvén-Coriolis modes.

We start by representing the perturbations up to a radius-dependent amplitude factor as follows:

$$f(r,\eta,t)=\exp[-i\lambda(r)t]\hat{f}(r,\eta),\tag{42}$$

where $\lambda(r)$ is the complex eigenvalue

$$\lambda=\Lambda+i\Gamma.\tag{43}$$

Substituting (42)-(43) into (36)-(41) results in the following system of linear ordinary differential equations for the perturbed velocity as well as in-plane magnetic field components. That system of equations characterizes the Alfvén-Coriolis waves and depends parametrically on the radius:

$$-i\lambda\hat{v}_r-2\hat{v}_\theta-\frac{1}{\bar{\beta}_z(r)\bar{\nu}(\eta)}\frac{d\hat{b}_r}{d\eta}=0,\tag{44}$$

$$-i\lambda\hat{v}_\theta+\frac{1}{2}\hat{v}_r-\frac{1}{\bar{\beta}_z(r)\bar{\nu}(\eta)}\frac{d\hat{b}_\theta}{d\eta}=0,\tag{45}$$

$$-i\lambda\hat{b}_r - \frac{d\hat{v}_r}{d\eta} = 0, \tag{46}$$

$$-i\lambda\hat{b}_\theta - \frac{d\hat{v}_\theta}{d\eta} + \frac{3}{2}\hat{b}_r = 0. \tag{47}$$

In addition, the Alfvén-Coriolis sub-system (44)-(47) is subject to the vanishing boundary conditions for the in-plane magnetic-field components.

The linear set of equations (44)-(47) may be reduced to the following single fourth order ordinary differential equations for both $\hat{b}_r$ and $\hat{b}_\theta$:

$$\frac{d}{d\eta}\left[\frac{1}{\bar{\nu}(\eta)}\frac{d^2}{d\eta^2}\left(\frac{1}{\bar{\nu}(\eta)}\frac{d\hat{b}_{r,\theta}}{d\eta}\right)\right] + (3+2\lambda^2)\bar{\beta}_z(r)\frac{d}{d\eta}\left(\frac{1}{\bar{\nu}(\eta)}\frac{d\hat{b}_{r,\theta}}{d\eta}\right) + \lambda^2(\lambda^2-1)\bar{\beta}_z^2(r)\hat{b}_{r,\theta} = 0. \tag{48}$$

Equation (48) is the same as the one used by Liverts & Mond (2009) who have derived it for a model problem under the assumption of zero radial variations of the perturbations. Here, it is important to emphasize however that the radial coordinate is a parameter a fact that renders the radial dependence of the perturbations arbitrary. Liverts & Mond (2009) have solved (48) with the aid of the Wentzel-Kramers-Brillouin (WKB) approximation for $\bar{\nu}(\eta) = \exp(-\eta^2/2)$. Remarkably, however, that a full analytical solution of Eq. (48) is possible for a slightly modified density profile. The first and main step towards that goal is to replace the isothermal density vertical steady-state distribution $\bar{\nu}(\eta) = \exp(-\eta^2/2)$ by the following function:

$$\bar{\nu}(\eta) = \mathrm{sech}^2(b\eta), \tag{49}$$

where the shape parameter b is determined by the requirement that the total mass of the disc does not change, namely:

$$\int_0^\infty \exp(-\eta^2/2)d\eta = \int_0^\infty \mathrm{sech}^2(b\eta)d\eta. \tag{50}$$

The result is:

$$b = \sqrt{2/\pi}. \tag{51}$$

The comparison of true and model number density profiles is presented in Fig. 1 and demonstrates a close correspondence between them. Furthermore, it will be shown below that the results derived by employing that profile are weakly distinguishable from the WKB results obtained for the true exponential distribution. In fact, notwithstanding the use of the terms true and model profiles, such a change of the equilibrium profile of the number density (that is determined by the axial momentum balance equation) may actually represent some true equilibrium that is obtained from a slightly different gravitational potential [see Spitzer (1942), where a similar density profile has been obtained as an exact solution for flat disc-galaxies whose disc mass content is larger than the mass of the central object].

Instead of Eq. (48) for the perturbed magnetic field it is more convenient to consider the equation for the perturbed velocity. Thus, substituting (49) - (51) into (44) - (47), yields the following ordinary differential equations for $\hat{v}_r$ and $\hat{v}_\theta$:

$$\frac{1}{\bar{\nu}(\eta)}\frac{d^2}{d\eta^2}\left(\frac{1}{\bar{\nu}(\eta)}\frac{d^2\hat{v}_{r,\theta}}{d\eta^2}\right) + (3+2\lambda^2)\bar{\beta}_z\frac{1}{\bar{\nu}(\eta)}\frac{d^2\hat{v}_{r,\theta}}{d\eta^2} + \lambda^2(\lambda^2-1)\bar{\beta}_z^2\hat{v}_{r,\theta} = 0. \tag{52}$$

The next step now is to introduce a new independent variable $\xi = \tanh(b\eta)$, such that $-1 \leqslant \xi \leqslant 1$. Doing that, a simpler equation emerges, which may be cast into the following form:

$$(L+K^-)(L+K^+)\hat{v}_\theta = 0, \tag{53}$$

where L is the Legendre operator of second order:

$$L = \frac{d}{d\xi}[(1-\xi^2)\frac{d}{d\xi}], \quad K^\pm = \frac{\bar{\beta}_z}{2b^2}[3+2\lambda^2 \pm \sqrt{9+16\lambda^2}].$$

Imposing now the zero boundary conditions of $\hat{b}_\theta$ at $\eta \to \infty$ leads to the requirement that the solution of Eq. (53) for $\hat{v}_\theta$ diverges polynomially at most when $\eta \to \infty$. It is concluded therefore that $\hat{v}_\theta$ is proportional to the Legendre polynomials $P_k(\xi)$ which are the solutions of the following equation:

$$\frac{d}{d\xi}\left((1-\xi^2)\frac{dP_k}{d\xi}\right) + K^\pm P_k, \quad K^\pm = k(k+1), \quad k = 1, 2, ... \tag{54}$$

Thus, the eigenvalues $\lambda^\pm$ are now determined by the dispersion relation

$$K^\pm \equiv \frac{\bar{\beta}_z(r)}{2b^2}[3+2\lambda^2 \pm \sqrt{9+16\lambda^2}] = k(k+1). \tag{55}$$

Employing now the recursive relations for the Legendre polinomyals:

$$(1-\xi^2)\frac{dP_k}{d\xi} = \frac{k(k+1)}{2k+1}[P_{k-1}(\xi) - P_{k+1}(\xi)],$$

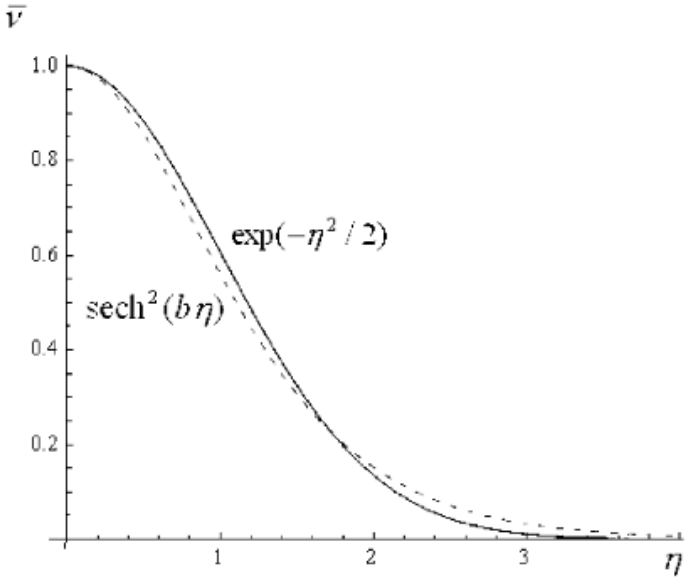

Figure 1. The comparison of true, $\bar{\nu} = \exp(-\eta^2/2)$ (solid) and model, $\bar{\nu} = \mathrm{sech}^2(b\eta)$ (dashed) number density profiles; $b = \sqrt{2/\pi}$.

setting the arbitrary amplitude of $\hat{v}_\theta$ to unity, and using the linear equations (44) - (47) result in the following expressions for the eigenfunctions that are determined up to an arbitrary radius dependent amplitude factor:

$$\hat{v}_r^{\pm} = i\lambda_a^{\pm}\left(\frac{1}{2} + \frac{3}{2}\frac{1}{\hat{\beta}_z}\frac{\hat{\beta}_z - 1}{(\lambda_a^{\pm})^2}\right) P_k(\xi), \quad \hat{v}_\theta^{\pm} = P_k(\xi),$$

$$\hat{b}_r^{\pm} = \frac{k(k+1)}{2k+1}\frac{b}{6}[(\lambda_a^{\pm}-1)(\lambda_a^{\pm}+1)\hat{\beta}_z - 3]\,[P_{k-1}(\xi) - P_{k+1}(\xi)],$$

$$\hat{b}_\theta^{\pm} = \frac{k(k+1)}{2k+1}\frac{b}{4}\frac{(1-\lambda_a^{\pm})(\lambda_a^{\pm}+1)\hat{\beta}_z - 1}{i\lambda_a^{\pm}}\,[P_{k-1}(\xi) - P_{k+1}(\xi)], \tag{56}$$

where $k = 1, 2, ...$ plays the role of axial wave number, $\hat{b}_\theta^{\pm} = 0$ for $\xi = \pm 1$, since $P_k(1) = 1$ and $P_k(-1) = (-1)^k$ for all k.

Turning back to the dispersion relation (58), it may be written as follows:

$$(\lambda^{\pm})^4\hat{\beta}_z^2 - (\lambda^{\pm})^2\hat{\beta}_z(\hat{\beta}_z + 6) + 9(1 - \hat{\beta}_z) = 0, \quad \hat{\beta}_z = \frac{\bar{\beta}_z}{\bar{\beta}_{cr}^{(k)}}. \tag{57}$$

It is thus obvious that the k-th mode is destabilized when the beta value crosses from bellow the threshold that is given by:

$$\bar{\beta}_{cr}^{(k)} = \frac{2}{3\pi}k(k+1). \tag{58}$$

As a result, a universal (for all values of $\bar{\beta}_z(r)$ and k) criterion for instability emerges which reads: $\hat{\beta}_z(r) > 1$. Written in terms of the scaled plasma beta $\hat{\beta}_z$ the dispersion relation (57) has the following solutions for the eigenvalues of the Alfvén-Coriolis modes (see Fig. 1):

$$\lambda^{\pm} = \sqrt{\frac{\hat{\beta}_z + 6 \pm \sqrt{(\hat{\beta}_z + 6)^2 - 36(1 - \hat{\beta}_z)}}{2\hat{\beta}_z}}. \tag{59}$$

The two eigenvalues, λ^+ and λ^-, represent fast and slow Alfvén-Coriolis waves. While the fast Alfvén-Coriolis modes are always stable, the number of unstable slow modes signified by the plasma beta. The eigenvalues of the slow Alfvén-Coriolis modes, λ^- , are given therefore by:

$$\lambda^- = \Lambda_a^- = \pm\sqrt{\frac{\hat{\beta}_z + 6 - \sqrt{(\hat{\beta}_z + 6)^2 - 36(1 - \hat{\beta}_z)}}{2\hat{\beta}_z}}, \ \mathrm{Im}\{\lambda^-\} = 0 \ \text{ for } \ \hat{\beta}_z \leqslant 1,$$

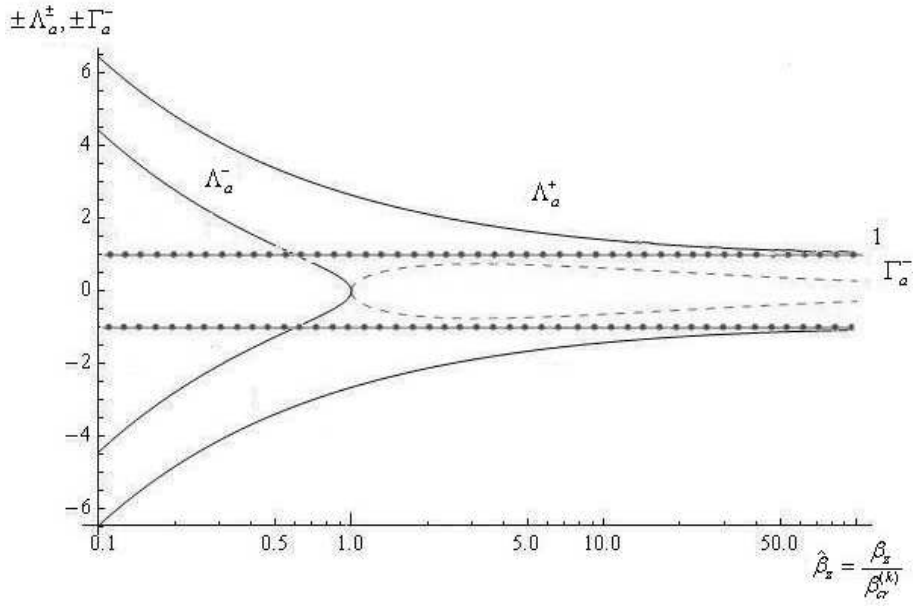

Figure 2. Growth rates $\pm\Gamma_a^-$ (dashed lines) for the unstable Alfvén-Coriolis (MRI) modes and frequencies $\pm\Lambda_a^{\pm}$ (solid lines) for the Alfvén-Coriolis oscillations vs universal scaled plasma beta, $\hat{\beta}_z = \bar{\beta}_z(r)/ = \bar{\beta}_{cr}^{(k)}$, $\bar{\beta}_{cr}^{(k)} = 2k(k+1)/(3\pi)$ for the model number density $\bar{\nu} = \mathrm{sech}^2(\sqrt{2/\pi}\eta)$; $k = 1, 2, \ldots$ is the axial wave number. Meshed straight-line asymptotes at $\hat{\beta}_z \gg 1$ are the scaled Keplerian frequencies, $\pm\Lambda_a^{\pm} = \pm 1$.

$$\lambda^- = i\Gamma_a^- = \pm i\sqrt{\frac{\sqrt{(\hat{\beta}_z+6)^2 + 36(\hat{\beta}_z - 1) - \beta_z} - 6}{2\hat{\beta}_z}}, \ \mathrm{Re}\{\lambda^-\} = 0 \ \text{ for } \ \hat{\beta}_z > 1. \tag{60}$$

The eigenvalues are imaginary, and the system is spectrally unstable if $\hat{\beta}_z > 1$, and real for $\hat{\beta}_z < 1$ in which case the system is stable. In particular, the minimal critical unscaled plasma beta that is needed for instability is determined by the first unstable slow Alfvén-Coriolis mode, $k = 1$, and is given by $\bar{\beta}_{cr}^{(1)} = 0.42$. The unstable modes are the well known MRIs and from Eq. (58) it is easy to calculate how many of them are excited for a given value of the plasma beta. Thus, there are k unstable modes for $\bar{\beta}_{cr}^{(1)} \leqslant \bar{\beta}_z(r) \leqslant \bar{\beta}_{cr}^{(k+1)}$. In particular, Eq. (58) yields approximately the square-root law for the number of the unstable modes vs plasma beta:

$$k < \sqrt{3\pi\bar{\beta}_z(r)/2}. \tag{61}$$

Relation (58) or its simplified version (61) is significant for the consequent modeling of non-linear development of the instability. It is finally emphasized that the stability criterion as well as the number of unstable modes depend on the radius. Thus, different areas within the disc may be characterized by different stability properties as well as different number of unbstable modes.

The family of the fast Alfvén-Coriolis modes, $\lambda^+(\hat{\beta}_z)$, is characterized by the frequencies that are much larger than the Keplerian frequency for small values of the scaled plasma beta (large values of axial wave number or small plasma beta) and tends to the Keplerian value at large plasma beta values:

$$\lambda^+ = \Lambda_a^+ = \pm\sqrt{\frac{\hat{\beta}_z + 6 + \sqrt{(\hat{\beta}_z+6)^2 - 36(1-\hat{\beta}_z)}}{2\hat{\beta}_z}}, \ \mathrm{Im}\{\lambda^+\} = 0. \tag{62}$$

Expressed in terms of the scaled plasma beta, a single figure depicts all possible stable as well as unstable modes. This is shown in Fig. 2. The maximal growth rate for the unstable modes is achieved around $\hat{\beta}_z \approx 3$, which for a given plasma beta value determines the axial wave number of the fastest growing modes.

Frequencies and growth rates for the first five fast and slow Alfvén-Coriolis modes are presented in Fig. 3 (in terms of the unscaled beta, $\bar{\beta}_z$). The corresponding growth rates Γ_a^- obtained by Liverts & Mond (2009) by employing the WKB approximation are weakly distinguishable from those in Fig. 3 and therefore are not shown on the figure. In particular, the critical plasma beta $\bar{\beta}_{cr}^{(1)}$ found by Liverts & Mond (2009) (after correction by factor 2 due to the different definition of the plasma beta there) is 0.417, which is practically the same as the one obtained in the current work.

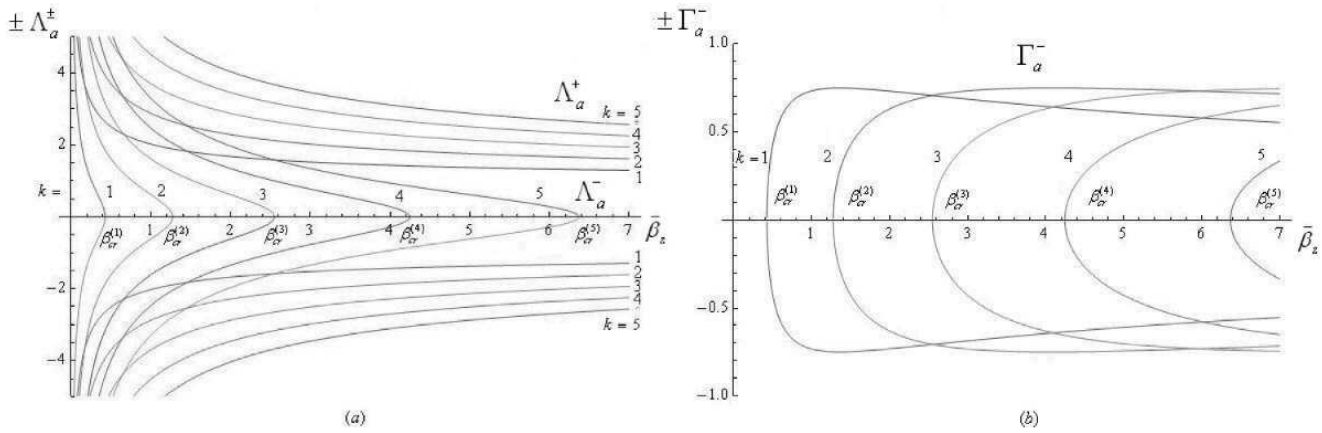

Figure 3. Frequencies $\pm\Lambda_a^{\pm}$ for the first five fast and slow Alfvén-Coriolis modes and growth rates $\pm\Gamma_a^-$ for the unstable (MRI) slow Alfvén-Coriolis modes vs unscaled plasma beta $\bar{\beta}_z$ for the model number density $\bar{\nu}=\mathrm{sech}^2(\sqrt{2/\pi}\eta)$; $\bar{\beta}_{cr}^{(k)}=2k(k+1)/(3\pi)$ is the critical plasma beta, $k=1,2,3,4,5$ is the axial wave number.

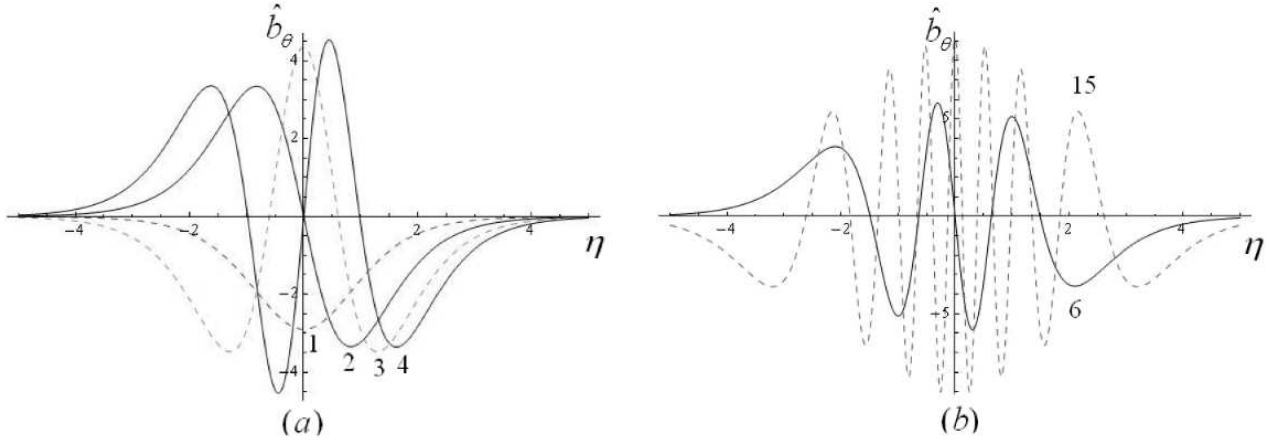

Figure 4. The toroidal component of the perturbed magnetic field $\hat{b}_\theta$ vs self-similar axial variable $\eta=z/H(r)$ for the Legendre polynomials with the axial wave numbers (a) $k=1,2,3,4$ and (b) $k=6$, 15. All curves are calculated for the fixed value of $\hat{\beta}_z=1.5$ ($\hat{\beta}_z=\bar{\beta}_z/\bar{\beta}_{cr}^{(k)}$, $\bar{\beta}_{cr}^{(k)}=b^2k(k+1)/3$, dashed and solid curves correspond to the odd and even k, respectively).

An illustration of the perturbed toroidal magnetic field is presented in Fig. 4. The perturbations are indeed localized within the effective height of the disc which weakly depends on the axial wave number. This corresponds to a finite distance between the turning points – the natural characteristics of the problem solution in the WKB approximation [Liverts & Mond (2009)]. To explicitly demonstrate the finite size of the region of perturbation's location, the differential equation for the perturbed magnetic field $\hat{b}_\theta$ in the self - similar variable η is written out:

$$\frac{d^2\hat{b}_\theta}{d\eta^2}+2b\xi\frac{d\hat{b}_\theta}{d\eta}+b^2K^{\pm}(1-\xi^2)\hat{b}_\theta=0,\quad \xi=\tanh(b\eta),\quad b=\sqrt{\frac{2}{\pi}},\quad K^{\pm}=k(k+1),\quad k=1,2,\ldots, \tag{63}$$

which is subject to zero boundary conditions at infinity. Equation (63) is derived by using differential equation (53) for $\hat{v}_\theta$ and a fact that $\hat{b}_\theta$ up to a constant coefficient of proportionality is equal to $d\hat{v}_\theta/d\eta$. Transforming as in WKB approximation the dependent variable $\hat{b}_\theta=Q(\eta)\int\mu(\eta)d\eta$, and setting $\mu(\eta)=-\xi=-\tanh(b\eta)$ in order to eliminate terms with first order derivatives yield:

$$\frac{d^2Q}{d\eta^2}+\varkappa^2(\eta)Q=0,\quad \varkappa^2(\eta)=b^2[K^{\pm}(1-\xi^2)-1]. \tag{64}$$

Then the turning points are determined from the relation $\varkappa^2(\eta)=0$, and may be found explicitly substituting $1-\xi^2$ by $\mathrm{sech}^2(b\eta)$:

$$\eta_*=b^{-1}\mathrm{arcsech}\frac{1}{\sqrt{k(k+1)}},\quad k=1,2,\ldots. \tag{65}$$

Table 3. Distances of the turning points from the midplane vs axial wave number.

k	1	2	3	4	5	6	15	35	155
η_*	1.1	1.9	2.4	2.7	3.0	3.2	4.3	5.3	7.2

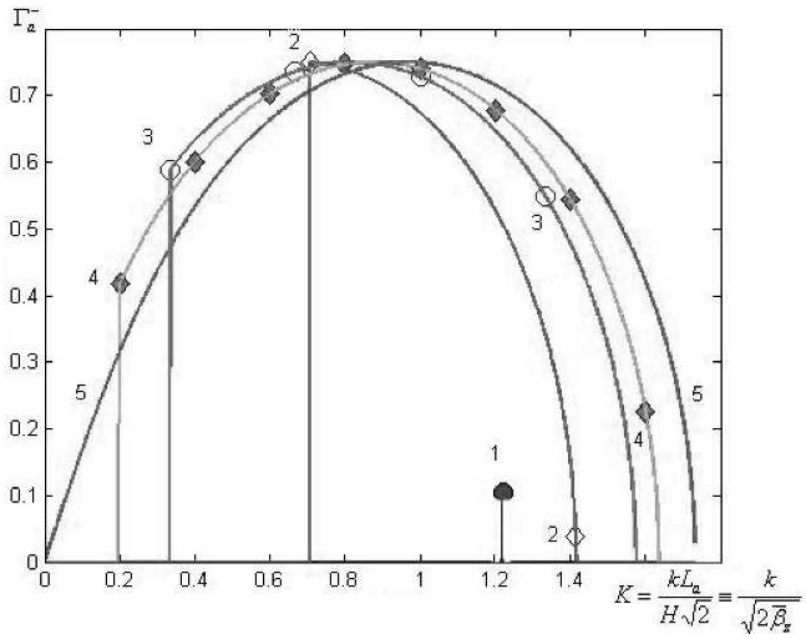

Figure 5. Growth rates Γ_a^- for the slow Alfvén-Coriolis modes vs effective wave number $K = \frac{kL_a}{H\sqrt{2}} \equiv \frac{k}{\sqrt{2\bar{\beta}_z}}$, $k = 1, 2, 3, ...$ is the number of the Alfvén-Coriolis modes, calculated for the model number density $\bar{\nu} = \mathrm{sech}(b\eta)$. Interpolating curves $1, 2, 3, 4, 5$ correspond to $\bar{\beta}_z = 0.41,\ 0.71,\ 1.5,\ 2.5,\ 500$, respectively.

The results for several axial wave numbers are presented in Table 3. Although the oscillation's region unboundedly expanded with rising axial wave numbers, this occurs very slowly and the region has relatively low sizes even at high values of k. Note that the unbounded growth which corresponds to high wave numbers should be suppressed by dissipative effects neglected in the present analysis.

In order to compare the current results to well known results for infinite homogeneous cylinders Balbus & Hawley (1991) the growth rate of the unstable modes is depicted in Fig. 5 as a function of the axial wave number K, where

$$K = k\frac{L_a}{H\sqrt{2}} \equiv \frac{k}{\sqrt{2\bar{\beta}_z}}, \tag{66}$$

$L_a = V_a/\Omega$ is the Alfvén length scale, $z = H\sqrt{2}$ is the effective height of the diffused disc at which the equilibrium number density, $\bar{n} \sim \exp[-z^2/(2H^2)]$, falls by factor e^{-1}. The effective wave number K is the discrete thin-disc analog of the continuous wave number for infinite cylindrical discs. For fixed value of the local plasma beta, $\bar{\beta}_z = 0.41,\ 0.5,\ 1.5,\ 2.5,\ 500$, the discrete set of the points in the plane $\{K, \Gamma_a^-\}$ is presented by one of the interpolating curves $1, 2, 3, 4, 5$, respectively. The number of the discrete points on each interpolating curves corresponds to the admissible values of the Alfvén-Coriolis mode number $k = 1, 2, 3, ...$ for which $\bar{\beta}_{cr}^{(1)} \leqslant \bar{\beta}_{cr}^{(k)} \leqslant \bar{\beta}_z(r)$. Also, the range of unstable k-values is widening as the value of $\bar{\beta}_z$ is increased. In particular, at large plasma beta the corresponding set of the points due to their large number (curve 5) should tend to the continuous curve for infinite cylinder geometry in Balbus & Hawley (1991). For finite plasma beta there is a discrete number of points on each curves in Fig. 5, where the left bound corresponds to the first Alfvén-Coriolis mode, $k = 1$. Thus, for beta values close to $\bar{\beta}_{cr}^{(1)}$, the number of unstable modes is small and the disk stability properties significantly deviate from those predicted by the infinite cylinder model.

3.4 Linear stability problem for magnetosonic modes

For simplicity it is assumed now that the poloidal component of the equilibrium magnetic field is zero and hence $\bar{\beta}_z = \infty$. Thus, substituting the exponential anzatz (42) into Eqs. (40) - (41) for the magnetosonic modes, and assuming that their frequencies are different from the eigenvalues of inertial-Coriolis waves yield:

$$-i\lambda\hat{v}_z+\frac{d}{d\eta}[\frac{\hat{\nu}}{\bar{\nu}(\eta)}]=0, \tag{67}$$

$$-i\lambda\frac{\hat{\nu}}{\bar{\nu}(\eta)}+\frac{d\hat{v}_z}{d\eta}+\frac{1}{\bar{\nu}(\eta)}\frac{d\bar{\nu}(\eta)}{d\eta}\hat{v}_z=0. \tag{68}$$

Since the effect of the magnetic field is dropped from the linear system (67) -(68), the latter actually describes sound waves that propagate vertically in the non-homogeneous disc. Eliminating the perturbed number density from (67) -(68) in the resulting equation yields a second order differential equation for the perturbed axial velocity:

$$\frac{d^2\hat{v}_z}{d\eta^2}+\frac{1}{\bar{\nu}(\eta)}\frac{d\bar{\nu}(\eta)}{d\eta}\frac{d\hat{v}_z}{d\eta}+\Big\{\lambda^2+\frac{d}{d\eta}\Big[\frac{1}{\bar{\nu}(\eta)}\frac{d\bar{\nu}(\eta)}{d\eta}\Big]\Big\}\hat{v}_z=0, \tag{69}$$

or substituting the equilibrium number density, $\bar{\nu}(\eta)=\exp(-\eta^2/2)$,

$$\frac{d^2\hat{v}_z}{d\eta^2}-\eta\frac{d\hat{v}_z}{d\eta}+(\lambda^2-1)\hat{v}_z=0. \tag{70}$$

Equation (70) is the Hermite equation and the requirement that its solutions diverges polynomially at most when $\eta\to\pm\infty$ determines the eigenvalues to be:

$$\lambda=\pm\Lambda_S=\pm\sqrt{m+1}, \tag{71}$$

while the eigenfunctions are given up to an amplitude factor depending on radius by:

$$\hat{v}_z=\mp i\sqrt{m+1}H_m(\eta),\ \ \hat{\nu}=e^{-\eta^2/2}H_{m+1}(\eta). \tag{72}$$

Here $H_m(\eta)$ $(m=1,2,\ )$ are the Hermite polynomials. The axial velocities are polynomially unbounded functions at $\eta\to\pm\infty$. Note that now the number of the Hermite polynomial m plays the role of the axial wave number for the magnetosonic mode that is different from the Alfvén-Coriolis modes with the number of the Legendre polynomial as the axial wave number. Formally, the above family of the solutions of the eigenvalue problem should be completed by the following degenerate steady-state solution:

$$\hat{\nu}=e^{-\eta^2/2},\ \ \hat{v}_z=0. \tag{73}$$

However, the latter may be considered as a modification of the unperturbed equilibrium solution.

4 DYNAMICAL EQUATIONS FOR PERTURBED THIN DISCS: TYPE II EQUILIBRIA

Consider now the thin disc problem under the effect of a dominant toroidal component of the equilibrium magnetic fields (see Tables 1 and 2). The solutions of such problem in the pure hydrodynamic case of zero magnetic field for adiabatic thin discs have been obtained and discussed in Shtemler et al. (2010) and are extended here for locally isothermal magnetized discs.

4.1 The reduced nonlinear equations

At this stage it is convenient to rescale all the physical variables, f, with the small parameter ϵ, without splitting the solution to its equilibrium and perturbed constituents. Thus, in a most general way, the physical variables are given by:

$$f(r,\zeta,t)=\epsilon^{S'}\tilde{f}(r,\zeta,t). \tag{74}$$

Here the auxiliary variables denoted by tilde are introduced, and the same orders, S', in ϵ are assumed for the physical variables as for the disturbed variables. For the dominant toroidal equilibrium magnetic field such choice is justified by the fact that any disturbed dependent variable is of the order of or larger than the corresponding equilibrium variable i.e. $S'\leqslant\bar{S}$ (see Tables 1 and 2). This imposes an additional limitation on the admissible time of perturbation growth. Substituting (74) into (2) -(6) yields up to the terms of the higher order in ϵ the following in-plane components of the momentum equation:

$$\frac{\partial\tilde{V}_r}{\partial t}+\tilde{V}_r\frac{\partial\tilde{V}_r}{\partial r}+\tilde{V}_z\frac{\partial\tilde{V}_r}{\partial\zeta}-\frac{\tilde{V}_\theta^2}{r}=-\frac{d\bar{\Phi}}{dr}, \tag{75}$$

$$\frac{\partial\tilde{V}_\theta}{\partial t}+\tilde{V}_r\frac{\partial\tilde{V}_\theta}{\partial r}+\tilde{V}_z\frac{\partial\tilde{V}_\theta}{\partial\zeta}+\frac{\tilde{V}_r\tilde{V}_\theta}{r}=0, \tag{76}$$

$$\frac{\partial\tilde{V}_z}{\partial t}+\tilde{V}_r\frac{\partial\tilde{V}_z}{\partial r}+\tilde{V}_z\frac{\partial\tilde{V}_z}{\partial\zeta}=-\frac{\bar{c}_S^2}{\tilde{n}}\frac{\partial\tilde{n}}{\partial\zeta}-\frac{\partial\bar{\phi}}{\partial\zeta}-\frac{1}{2\beta\tilde{n}}\frac{\partial(\tilde{B}_\theta^2+\tilde{B}_r^2)}{\partial\zeta}, \tag{77}$$

$$\frac{\partial\tilde{n}}{\partial t}+\frac{1}{r}\frac{\partial(r\tilde{n}\tilde{V}_r)}{\partial r}+\frac{\partial(\tilde{n}\tilde{V}_z)}{\partial\zeta}=0, \tag{78}$$

$$\frac{\partial \tilde{B}_r}{\partial t} - \frac{\partial \tilde{E}_\theta}{\partial \zeta} = 0, \tag{79}$$

$$\frac{\partial \tilde{B}_\theta}{\partial t} + \frac{\partial \tilde{E}_r}{\partial \zeta} - \frac{\partial \tilde{E}_z}{\partial r} = 0, \tag{80}$$

$$\frac{\partial \tilde{B}_z}{\partial t} + \frac{1}{r}\frac{\partial (r\tilde{E}_\theta)}{\partial r} = 0. \tag{81}$$

Here

$$\tilde{E}_r = \tilde{V}_z\tilde{B}_\theta - \tilde{V}_\theta\tilde{B}_z, \;\; \tilde{E}_\theta = \tilde{V}_r\tilde{B}_z - \tilde{V}_z\tilde{B}_r, \;\; \tilde{E}_z = \tilde{V}_\theta\tilde{B}_r - \tilde{V}_r\tilde{B}_\theta. \tag{82}$$

The system (75)- (82) is subject the boundary conditions at infinity of least possible divergence for the axial velocity and the vanishing of the in-plane magnetic-field components.

4.2 The linearized problem

We start by linearizing the MHD equations (75) - (82) about the steady-state equilibrium solution (12) - (15). Substituting the decomposition of the total disturbed variables (18) into Eqs. (75) - (82), yields the following linear set of equations for axisymmetric perturbations:

$$\frac{\partial V_r'}{\partial t} - 2\bar{\Omega}(r)V_\theta' = 0, \tag{83}$$

$$\frac{\partial V_\theta'}{\partial t} + \frac{1}{2}\bar{\Omega}(r)V_r' = 0, \tag{84}$$

and

$$\frac{\partial V_z'}{\partial t} + \bar{c}_S^2(r)\frac{\partial}{\partial \zeta}(\frac{n'}{\bar{n}}) + \frac{1}{\beta}\frac{\bar{B}_\theta(r)}{\bar{n}}\frac{\partial B_\theta'}{\partial \zeta} = 0, \tag{85}$$

$$\frac{\partial n'}{\partial t} + \frac{\partial (\bar{n}V_z')}{\partial \zeta} = -\frac{1}{r}\frac{\partial (r\bar{n}V_r')}{\partial r}, \tag{86}$$

$$\frac{\partial B_r'}{\partial t} = \bar{B}_z(r)\frac{\partial V_r'}{\partial \zeta}, \tag{87}$$

$$\frac{\partial B_\theta'}{\partial t} + \bar{B}_\theta(r)\frac{\partial V_z'}{\partial \zeta} = r\frac{d\bar{\Omega}}{dr}B_r' + \bar{B}_z(r)\frac{\partial V_\theta'}{\partial \zeta} - \frac{\partial [\bar{B}_\theta(r)V_r']}{\partial r}. \tag{88}$$

As for the equilibria type I, the equation for the perturbed magnetic field, B_r', is obtained by differentiating by the equation for the magnetic flux function, Ψ', while the corresponding equation for the perturbed axial magnetic field, B_z', decouples from the rest of the equations, and drops out altogether from the governing system (83)-(88). As in the case of comparable axial and toroidal magnetic field components (type I equilibria), also the reduced linear system (83)-(88) is decoupled into two linear sub-systems that describe now the dynamics of the inertial-Coriolis (IC), $\{V_r', v_\theta'\}$, and magnetosonic (MS), $\{V_z',\, n',\, B_r',\, B_\theta',\, B_z'\}$, modes. A notable difference between the two cases however is that, while for the type I equilibria the radial derivatives drop out altogether from the reduced nonlinear system of equations, in the current case, some of the radial derivatives do survive the asymptotic procedure, due to the relative smallness of the axial magnetic field component. As will be shown later on, this difference turns out to be quite significant as the radial derivatives are responsible for the non modal algebraic growth of the initially small perturbations.

Back to the modes of wave propagation, the IC waves are described by Eqs. (83) and (84) while the MS modes are given by the solution of the homogeneous parts of Eqs. (85)-(88). Also, the perturbed radial magnetic field, B_r', is completely determined by the perturbed radial velocity, V_r', and hence Eq. (87) is separated from the rest of the magnetosonic sub-system. The right hand sides of Eqs. (86) and (88) result in the (resonant as well as nonresonant) forcing of the MS waves by the IC modes. As will be seen later on, this occurs due to the rotational shear.

Before actually solving the above linearized system of equations it is noted that, guided by the steady-state solution, it is convenient to introduce the following new independent variables:

$$\theta = t, \;\; \rho = \int_0^r \frac{dr}{\bar{H}(r)}, \;\; \eta = \frac{\zeta}{\bar{H}(r)}, \;\; (\bar{H}(r) = \frac{\bar{c}_S(r)}{\bar{\Omega}(r)}). \tag{89}$$

Then derivatives in new and old variables are related as follows:

$$\frac{\partial}{\partial t} = \frac{\partial}{\partial \theta}, \;\; \frac{\partial}{\partial \zeta} = \frac{1}{\bar{H}}\frac{\partial}{\partial \eta}, \;\; \frac{\partial}{\partial r} = \frac{\partial}{\partial \rho} - \frac{1}{\bar{H}^2}\frac{d\bar{H}}{d\rho}\eta\frac{\partial}{\partial \eta}. \tag{90}$$

Equations (83)-(88) may be rewritten by introducing the following scaled variables:

$$\mathbf{v}(\rho,\eta,\theta)=\frac{\mathbf{V}'}{\bar{c}_S(r)},\ \ \nu(\rho,\eta,\theta)=\frac{n'}{\bar{N}(r)},\ \ \mathbf{b}(\rho,\eta,\theta)=\frac{\mathbf{B}'}{\bar{B}_\theta(r)}. \tag{91}$$

Below for convenience and with no confusion we revert to the notation t for the new variable θ. This yields the following system of equations:

$$\frac{1}{\bar{\Omega}}\frac{\partial v_r}{\partial t}-2v_\theta=0, \tag{92}$$

$$\frac{1}{\bar{\Omega}}\frac{\partial v_\theta}{\partial t}+\frac{1}{2}v_r=0, \tag{93}$$

and

$$\frac{1}{\bar{\Omega}}\frac{\partial v_z}{\partial t}+\frac{\partial}{\partial\eta}[\frac{\nu}{\bar{\nu}(\eta)}]+\frac{1}{\bar{\beta}_\theta\bar{\nu}(\eta)}\frac{\partial b_\theta}{\partial\eta}=0, \tag{94}$$

$$\frac{1}{\bar{\Omega}}\frac{\partial}{\partial t}[\frac{\nu}{\bar{\nu}(\eta)}]+\frac{\partial v_z}{\partial\eta}-\eta v_z=-\frac{\partial v_r}{\partial\rho}-\bar{D}_N v_r+\bar{D}_\Omega(\frac{\partial v_r}{\partial\eta}-\eta v_r)\eta, \tag{95}$$

$$\frac{1}{\bar{\Omega}}\frac{\partial b_r}{\partial t}=\frac{1}{\bar{S}(r)}\frac{\partial v_r}{\partial\eta}, \tag{96}$$

$$\frac{1}{\bar{\Omega}}\frac{\partial b_\theta}{\partial t}+\frac{\partial v_z}{\partial\eta}=-\frac{\partial v_r}{\partial\rho}-\frac{3}{2}b_r+\frac{1}{\bar{S}(r)}\frac{\partial v_\theta}{\partial\eta}-\bar{D}_B v_r+\bar{D}_\Omega\frac{\partial v_r}{\partial\eta}\eta. \tag{97}$$

Here $\bar{\beta}_\theta(\rho)$, $\bar{\beta}_z(\rho)$ and $\bar{S}(r)$ are given by (35); $\bar{\beta}_\theta(\rho)$ and $\bar{\beta}_z(\rho)$ are proportional to the characteristic lasma beta, β, that is now based on the dimensional toroidal component of the equilibrium magnetic field as the characteristic scale, $B_*=B_\theta(r_*)$; $\bar{D}_N(\rho)$, $\bar{D}_\Omega(\rho)$ and $\bar{D}_B(\rho)$ are the following logarithmic derivatives:

$$\bar{D}_N=\frac{d\ln(\bar{c}_S r\bar{N})}{d\rho},\ \ \bar{D}_\Omega=\frac{d\ln(\bar{c}_S/\bar{\Omega})}{d\rho}\equiv\frac{d\ln\bar{H}}{d\rho},\ \ \bar{D}_B=\frac{d\ln(\bar{c}_S\bar{B}_\theta)}{d\rho}. \tag{98}$$

A single equation for the magnetosonic modes may be derived now by eliminating the toroidal component of the perturbed magnetic field as well as the perturbed number density from Eqs. (94) - (97). The result is:

$$\frac{1}{\bar{\Omega}^2}\frac{\partial^2 v_z}{\partial t^2}-(1+\frac{1}{\bar{\beta}_\theta\bar{\nu}(\eta)})\frac{\partial^2 v_z}{\partial\eta^2}+\eta\frac{\partial v_z}{\partial\eta}+v_z=\frac{1}{\bar{\beta}_\theta\bar{\nu}(\eta)}(\frac{3}{2}\frac{\partial b_r}{\partial\eta}-\sqrt{\frac{\bar{\beta}_\theta}{\bar{\beta}_z}}\frac{\partial^2 v_\theta}{\partial\eta^2})+(1+\frac{1}{\bar{\beta}_\theta\bar{\nu}(\eta)})\frac{\partial^2 v_r}{\partial\eta\partial\rho}+L_z v_r, \tag{99}$$

where L_z is the linear ordinary differential operator:

$$L_z v_r=\bar{D}_N\frac{\partial v_r}{\partial\eta}-\bar{D}_\Omega[(1+\frac{1}{\bar{\beta}_\theta\bar{\nu}(\eta)})\frac{\partial}{\partial\eta}(\eta\frac{\partial v_r}{\partial\eta})-\frac{\partial(\eta^2 v_r)}{\partial\eta}]+\bar{D}_B\frac{1}{\bar{\beta}_\theta\bar{\nu}(\eta)}\frac{\partial v_r}{\partial\eta}. \tag{100}$$

Note that in the important particular case of pure hydrodynamic discs the equilibrium and perturbed components of the magnetic field should be set to zero, i.e. $\bar{\beta}_\theta=\bar{\beta}_z=\infty$ and $b_r=b_\theta=0$, then Eqs. (97) - (98) with the properly resolved uncertainty in $\bar{\beta}_\theta/\bar{\beta}_z$ are satisfied identically, and Eq. (99) is replaced by

$$\frac{1}{\bar{\Omega}^2}\frac{\partial^2 v_z}{\partial t^2}-\frac{\partial^2 v_z}{\partial\eta^2}+\eta\frac{\partial v_z}{\partial\eta}+v_z=\frac{\partial^2 v_r}{\partial\eta\partial\rho}+\bar{D}_N\frac{\partial v_r}{\partial\eta}-\bar{D}_\Omega[\frac{\partial}{\partial\eta}(\eta\frac{\partial v_r}{\partial\eta})-\frac{\partial(\eta^2 v_r)}{\partial\eta}]. \tag{101}$$

The above problems formulated for the magnetized and magnetic-field free discs are complemented by the boundary condition of least possible divergence at infinity for the axial velocity, and in the case of magnetized discs the vanishing conditions for the in-plane magnetic-field components should be also satisfied.

An important result is immediately seen from the above set of linearized equations: to leading order in ϵ: Eqs. (92)-(93) decouple from the rest of the system in the thin disc approximation. Note additionally that Eq. (96) for the radial magnetic field, explicitly determined by the radial velocity, may be solved separately from the rest Alfvén-mode sub-system. Thus, the sub-system (91)-(92) describes pure hydrodynamic in-plane inertia-Coriolis waves, and signifies the decoupling of the latter from the Alfvén waves. This occurs due to the negligibly small values of the projections on the disc plane of the pressure gradient and Lorentz force in the momentum balance equations (of the order of ϵ^2) compared with the inertial terms (of the order of ϵ^0) in the thin disc approximation. Thus, in the case of poloidal-dominated equilibrium, the magnetic field is of order ϵ^0 which renders the Lorentz force of the same order of magnitude as the inertial terms, and thus couples the Lorentz and inertia forces. This results in the coupling of the Coriolis and Alfvén waves that eventually leads to the MRI. In contrast, the case of the toroidal-dominated magnetic field inevitably results in the scaling $\bar{B}_z\sim\epsilon$. This, as indicated above, means that the radial and azimuthal components of the Lorentz force are negligible with respect to the corresponding components of the inertial forces in the radial and azimuthal components of the momentum equation. As is already apparent, that decoupling between the inertial and Lorentz forces causes to a crucial deviation from the former case (i.e., with polidal-dominated equilibrium magnetic field) and leads to the removal of the mechanism that is responsible to the MRI.

4.3 Linear stability problem.

The perturbations may be presented as follows

$$f(\rho,\eta,t)=\exp[-i\lambda\bar{\Omega}(\rho)t]\hat{f}(\rho,\eta), \tag{102}$$

where $\lambda=\omega/\bar{\Omega}$ is the scaled frequency.

Inertia-Coriolis modes. Substituting (102) into (92) - (93) yields:

$$-i\lambda\hat{v}_r-2\hat{v}_\theta=0, \tag{103}$$

$$-i\lambda\hat{v}_\theta+\frac{1}{2}\hat{v}_r=0. \tag{104}$$

The corresponding dispersion relation is therefore given by

$$\lambda=\pm 1, \tag{105}$$

which represents, the stable epicyclical oscillations in the disc plane, since for Keplerian rotation, the epicyclical frequency equals to Keplerian one, $\bar{\chi}(\rho)=\bar{\Omega}(\rho)$. As ρ and η are mere parameters each ring $\rho=const$, $\eta=const$ vibrates independently in its own plane. If viscous stresses are taken into account, an axial profile is imposed due to the mutual shear stresses between the rings and each entire cylindrical shell vibrates independently. This is indeed the case that has been solved in [Umurhan et al. (2006); Rebusco et al. (2009)); Shtemler et al. (2010)]. As the axial and radial coordinates play the role of passive parameters, the eigenfunctions of the inertia-Coriolis modes are determined up to arbitrary amplitude $A(\rho,\eta)$ from (103)-(105):

$$\hat{v}_\theta=\mp i\frac{1}{2}\hat{v}_r=\mp i\frac{1}{2}A(\rho,\eta). \tag{106}$$

Since any special form of the function represents some given set of initial conditions, the following self-similar separable form of the planar velocities is considered as an example:

$$A(\rho,\eta)=F(\rho)G(\eta), \tag{107}$$

where the $F(\rho)$ and $G(\eta)$ are arbitrary functions.

Magnetosonic modes. For frequencies that are different from the eigenvalues of inertial waves, namely $\lambda\equiv\omega/\Omega(\rho)=\pm 1$ in (105), both the perturbed in-plane components of the velocity as well as the radial component of the perturbed magnetic field are zero, i.e. $\hat{v}_r=\hat{v}_\theta=\hat{b}_r\equiv 0$. Therefore, the perturbed axial velocity, number density, as well as the toroidal magnetic field are described by the set of equations that governs the dynamics of the magnetosonic waves:

$$[1+\frac{1}{\bar{\beta}_\theta\bar{\nu}(\eta)}]\frac{d^2\hat{v}_z}{d\eta^2}-\eta\frac{d\hat{v}_z}{d\eta}+(\lambda^2-1)\hat{v}_z=0, \tag{108}$$

$$-i\lambda\frac{\hat{\nu}}{\bar{\nu}(\eta)}+\frac{d\hat{v}_z}{d\eta}-\eta\hat{v}_z=0, \tag{109}$$

$$-i\lambda\hat{b}_\theta+\frac{d\hat{v}_z}{d\eta}=0, \tag{110}$$

is subject to the boundary conditions at infinity of the least possible divergence for the axial velocity and the vanishing conditions for the in-plane magnetic-field components. Partial solutions are presented below .

(i) The pure hydrodynamic system. First start with a simple exact solution for the pure hydrodynamic system. Accounting to Eq. (101) this yields

$$\frac{d^2\hat{v}_z}{d\eta^2}-\eta\frac{d\hat{v}_z}{d\eta}+(\lambda^2-1)\hat{v}_z=0, \tag{111}$$

$$-i\lambda\frac{\hat{\nu}}{\bar{\nu}(\rho)}+\frac{d\hat{v}_z}{d\eta}-\eta\hat{v}_z=0, \tag{112}$$

complemented by the boundary condition of least possible divergence at infinity for the axial velocity. That problem is degenerated to the sound waves, and coincides with the case of the poloidal-dominated equilibrium magnetic field, and its solution is:

$$\lambda=\pm\Lambda_S=\pm\sqrt{m+1},\ \ \hat{v}_z=-i\lambda W(\rho)H_m(\eta),\ \ \frac{\hat{\nu}}{\bar{\nu}}=W(\rho)H_{m+1}(\eta)\quad \text{at}\ \ \eta=\pm\infty. \tag{113}$$

Here λ are the radius-independent eigenvalues; $W(\rho)$ are the radius-dependent amplitude factors; $H_m(\eta)$, $m=0,1,2,...$ are the Hermite polynomials.

(ii) The limit of large plasma beta in magnetized discs. The WKB approximation is employed now. In general, it may be applied for a wide range of plasma beta values. However, in order to simplify calculations, we restrict ourselves here by

its application to the limit of large but finite values of the plasma beta. Such approach is necessary as a simple asymptotic expansion in large plasma beta $\bar{\beta}_\theta$ fails at large η (small $\bar{\nu}(\eta)$) due to the non-uniform limit of $\bar{\beta}_\theta\bar{\nu}(\eta)$ in Eq. (108). As a first step the following equation for $\hat{b}_\theta$ is derived from the system (108) - (110)

$$\frac{d^2\hat{b}_\theta}{d\eta^2}-\eta\frac{\bar{\beta}_\theta^2\bar{\nu}(\eta)-1}{\bar{\beta}_\theta^2\bar{\nu}(\eta)+\bar{\beta}_\theta}\frac{d\hat{b}_\theta}{d\eta}+(\lambda^2-1)\frac{\bar{\beta}_\theta\bar{\nu}(\eta)}{1+\bar{\beta}_\theta\bar{\nu}(\eta)}\hat{b}_\theta=0, \tag{114}$$

with the following boundary conditions:

$$\hat{b}_\theta=0 \qquad \text{at} \quad \eta=\pm\infty. \tag{115}$$

To reduce Eq. (114) to the form appropriate for WKB approximation, the dependent variable is transformed in the following way in order to eliminate terms with first order derivatives:

$$\hat{b}_\theta=Q\int\mu d\eta, \quad \mu=\frac{\eta}{2\bar{\beta}_\theta}\frac{\bar{\beta}_\theta^2\bar{\nu}(\eta)-1}{\bar{\beta}_\theta\bar{\nu}(\eta)+1}. \tag{116}$$

Then

$$\frac{d^2Q}{d\eta^2}+\varkappa^2(\eta)Q=0, \tag{117}$$

where

$$\varkappa^2(\eta)=-\eta^2\frac{1+\bar{\beta}_\theta}{2\bar{\beta}_\theta}\frac{\bar{\beta}_\theta\bar{\nu}(\eta)}{[1+\bar{\beta}_\theta\bar{\nu}(\eta)]^2}-\frac{1}{2\bar{\beta}_\theta}\frac{1-\bar{\beta}_\theta^2\bar{\nu}(\eta)}{1+\bar{\beta}_\theta\bar{\nu}(\eta)}-\eta^2\frac{1}{4\bar{\beta}_\theta^2}[\frac{1-\bar{\beta}_\theta^2\bar{\nu}(\eta)}{1+\bar{\beta}_\theta\bar{\nu}(\eta)}]^2+(\lambda^2-1)\frac{\bar{\beta}_\theta\bar{\nu}(\eta)}{1+\bar{\beta}_\theta\bar{\nu}(\eta)}. \tag{118}$$

The approximate solutions appropriate to real and imagine $\varkappa(\eta)$, at which the solution oscillates and decrease, respectively, are as follows (see e.g. Migdal (1977)):

$$Q=\frac{W}{\sqrt{\varkappa(\eta)}}\exp(\pm i\int\varkappa(\eta)d\eta \quad \text{and} \quad Q=\frac{W}{\sqrt{\mid\varkappa(\eta)\mid}}\exp(\pm\int\mid\varkappa(\eta)\mid d\eta. \tag{119}$$

The regions of each of the solutions given in Eq. (119) are determined by the turning points which are the zeros of $\varkappa(\eta)$. It can be easily seen that large-plasma beta approximation is uniformly valid in the region between the turning points, and violated at large η due to uncertainty in the term $\bar{\beta}_\theta\bar{\nu}(\eta)$ in (118) for exponentially vanishing $\bar{\nu}(\eta)=\exp(-\eta^2/2)$ at $\eta\to\pm\infty$ and $\bar{\beta}_\theta\sim\beta\gg1$. Since application of the WKB method is justified asymptotically at large frequency λ, Eq. (118) is considered for large but fixed values of $\bar{\beta}_\theta$ and λ, and for such large η that both $\bar{\beta}_\theta\bar{\nu}(\eta)$ and $\bar{\beta}_\theta^2\bar{\nu}(\eta)$ are small. Then Eq. (118) yields to leading order

$$\varkappa^2(\eta)\approx-\frac{1}{2\bar{\beta}_\theta}(1+\frac{\eta^2}{2\bar{\beta}_\theta}), \quad \mu(\eta)\approx-\frac{1}{2\bar{\beta}_\theta}\eta. \tag{120}$$

Choosing the minus sign to satisfy the boundary condition (115) in the approximate solution (119) for $\mid\eta\mid>\mid\eta_*\mid$, yields the following form for sufficiently large η:

$$\hat{b}_\theta\sim\frac{1}{\mid\varkappa\mid}\exp(-\frac{\eta^2}{4\bar{\beta}_\theta}\pm\int_{\eta_*}^{\eta}\mid\varkappa\mid d\eta)=\frac{2\bar{\beta}_\theta}{\eta^2}\exp(-\frac{\eta^2}{2\bar{\beta}_\theta}). \tag{121}$$

To further simplify the calculations, assume additionally that $\bar{\beta}_\theta\gg1$, then the large beta limit is uniformly valid within the interval $\mid\eta\mid\leqslant\mid\eta_*\mid$, and $\varkappa$ and μ are given by

$$\varkappa^2(\eta)\approx-\frac{1}{4}(\eta^2-\eta_*^2), \quad \mu(\eta)\approx\frac{1}{2}\eta, \tag{122}$$

where $\eta_*=\pm\sqrt{4\lambda^2-2}$ are the turning points of the equation (117) which separate the regions of oscillatory and exponentially decreasing behavior of the solution. Thus, $\varkappa=0$ at $\mid\eta\mid=\mid\eta_*\mid$, $\varkappa^2$ is positive within the inner region$\mid\eta\mid\leqslant\mid\eta_*\mid$ and negative otherwise within the outer region. To completely determine the problem solution, the conventional WKB approximation applies the matching conditions to the solutions (119) in the inner ($\mid\eta\mid\leqslant\mid\eta_*\mid$) and outer ($\mid\eta\mid\geqslant\mid\eta_*\mid$) regions in order to obtain the coefficients in (119) and the eigenvalue equation. The result is the following Bohr-Zommerfeld condition [Landau & Lifshits (1997)] that determines the dispersion relation

$$\int_{-\eta_*}^{+\eta_*}\varkappa d\eta=\pi(m+\frac{1}{2}), \tag{123}$$

where $\varkappa$ is given by (122), and m is the number of zeros of the solution within the inner region. Substituting (122) into (123) yields

$$\lambda=\pm\sqrt{m+1}. \tag{124}$$

The eigenvalues (124) exactly coincide with those in (113) obtained with no restrictions on the value of axial wave numbers m for the pure hydrodynamic system.

Finally note that although the WKB method is valid asymptotically for large frequencies, $\lambda \gg 1$ (i.e. large plasma beta or, alternatively, large axial wave numbers, m), it frequently yields a fair approximation up to finite values $\lambda \sim 1$ [see e.g. Migdal (1977)]. This allows expecting that eigenvalues (124) will be appropriate even for low axial wave numbers $m = 1, 2, \ldots$.

(iii) The limit of small plasma beta in magnetized discs. Consider the problem (108) -(110) in the limit of small plasma beta $\bar{\beta}_\theta(\rho) \sim \bar{\beta} \ll 1$. Assuming simultaneously that the eigenvalue λ is large, so that $\lambda^2\bar{\beta}_\theta \sim \bar{\beta}^0$, Eq. (108) yields to leading order in small $\bar{\beta}$

$$\frac{d^2\hat{v}_z}{d\eta^2} + \lambda^2\bar{\beta}_\theta\bar{\nu}(\eta)\hat{v}_z = 0. \tag{125}$$

Replacing as in Section 3.3 the steady-state isothermal density distribution $\bar{\nu}(\eta) = \exp(-\eta^2/2)$ by the hyperbolic function $\bar{\nu}(\eta) = \mathrm{sech}^2(b\eta)$ with $b = \sqrt{2/\pi}$, and introducing the auxiliary variable $\xi = \tanh(b\eta)$, transform Eq. (125) to the following form:

$$L\hat{v}_z + \bar{\lambda}^2\hat{v}_z = 0, \tag{126}$$

where L is the Legendre differential operator of second order,

$$L \equiv \frac{d}{d\xi}[(1-\zeta^2)\frac{d}{d\xi}],$$

and $\bar{\lambda}^2$ is given by:

$$\bar{\lambda}^2 = \frac{1}{b^2}\lambda^2(\rho)\bar{\beta}_\theta(\rho) \sim \bar{\beta}^0. \tag{127}$$

Imposing now that $\hat{v}_z$ diverges polynomially at most when $\eta \to \infty$, leads to the conclusion that the solution of Eq. (127) for $\hat{v}_z$ is proportional to the Legendre polynomials $P_m(\xi)$:

$$\frac{\hat{v}_z}{W(\rho)} = P_m(\xi) \sim \bar{\beta}^0, \quad \bar{\lambda}^2 = m(m+1) \sim \bar{\beta}^0, \quad m = 1, 2, ... \tag{128}$$

Equations (106) - (107) yield that $\hat{b}_\theta$ and $\hat{\nu}$ are of higher order in small plasma beta:

$$\frac{\hat{b}_\theta}{W(\rho)} = -i\sqrt{\frac{m}{m+1}}[P_{m-1}(\xi) - \xi P_m(\xi)]\bar{\beta}_\theta^{1/2} \sim \bar{\beta}^{1/2},$$

$$\frac{\hat{\nu}}{W(\rho)} = \frac{i}{b}\sqrt{\frac{m}{m+1}}(1-\xi^2)[(\xi + \frac{1}{mb}\mathrm{arctanh}\xi)P_m(\xi) - P_{m-1}(\xi)]\bar{\beta}_\theta^{1/2} \sim \bar{\beta}^{1/2}. \tag{129}$$

Since $P_m(1) = 1$ and $P_m(-1) = (-1)^m$ for all m, $\hat{b}_\theta$ satisfies the vanishing boundary condition at infinity $\eta \to \pm\infty$ ($\xi \to \pm 1$).

Thus, summarizing, the main conclusion from both limits (high and low plasma beta) is that the inertia-Coriolis waves are decoupled from the Alfvén waves, which henceforth leads to the complete stabilization of the MRI's. This, as will be subsequently seen, leaves the stage exclusively to the non modal algebraic growth mechanism. Remarkably that both limits assume sufficiently large values of the eigenvalues (scaled frequensies λ): in the limit of large β in (124) due to high frequency assumption inherent to WKB, while in opposite limit of small β in (128), because to asymptotic behavior of $\lambda \sim \beta^{-1/2}$.

4.4 Non-resonantly and resonantly driven magnetosonic modes

There are two mechanisms responsible for algebraic time-growth of perturbations, namely non-resonant and resonant excitation of vertical magnetosonic waves by planar inertia-Coriolis modes. This fact for the pure hydrodynamic adiabatic discs was established in [Umurhan et al. (2006); Rebusco et al. (2009)); Shtemler et al. (2010)]. As shown below, both mechanisms are also relevant in a modified form for vertically-isothermal magnetized discs. Due to the rotation shear effect and the presence of radial derivatives in the system (95) -(101), the amplitude of the magnetosonic modes driven by the inertia-Coriolis modes grows linearly in time in the case when the magnetosonic mode frequency is not equals to the inertial-Coriolis one. While for the same frequencies of the magnetosonic and inertial-Coriolis modes, the latter grows quadratically in time.

To demonstrate linear and quadratic in time growth of the perturbations, both non-resonantly and resonantly driven modes are illustrated below by simple explicit solutions. The non-resonantly driven magnetosonic waves are considered in the limit of small toroidal plasma beta and for pure hydrodynamic system, as typical examples. Noting that the resonantly driven magnetosonic modes may exist for arbitrary frequencies, we restrict ourselves by considering a pure hydrodynamic system which is characterized by simple explicit solutions with no limitation on the frequency value.

The driving modes are characterized by Eqs. (102) and (106). As a result, the driven magnetosonic or sound modes in magnetized or magnetic-field free discs, i.e. (99) or (101), respectively, are described by the following expressions:

$$\{v_r,\ v_\theta,\ b_\theta\} = \exp[-i\lambda\bar{\Omega}(\rho)t]\{\hat{v}_r,\ \hat{v}_\theta,\ \hat{b}_\theta\}(\rho,\eta,t). \tag{130}$$

Inserting then Eq. (130) into the system of equations ((94)-((101) and keeping only terms that are proportional to t on their right hand sides yield

$$\frac{1}{\bar{\Omega}^2}\frac{\partial^2 v_z}{\partial t^2} - (1+\frac{1}{\bar{\beta}_\theta\bar{\nu}(\eta)})\frac{\partial^2 v_z}{\partial\eta^2} + \eta\frac{\partial v_z}{\partial\eta} + v_z = \mp it\exp[-i\lambda\bar{\Omega}(\rho)t](1+\frac{1}{\bar{\beta}_\theta\bar{\nu}(\eta)})\frac{d\bar{\Omega}}{d\rho}\frac{\partial\hat{v}_r}{\partial\eta}, \tag{131}$$

$$\frac{1}{\bar{\Omega}}\frac{\partial}{\partial t}[\frac{\nu}{\bar{\nu}(\eta)}] + \frac{\partial v_z}{\partial\eta} - \eta v_z = \pm it\exp[\mp i\bar{\Omega}(\rho)t]\,\frac{d\bar{\Omega}}{d\rho}\hat{v}_r, \tag{132}$$

$$\frac{1}{\bar{\Omega}}\frac{\partial b_\theta}{\partial t} + \frac{\partial v_z}{\partial\eta} = \pm it\exp[\mp i\bar{\Omega}(\rho)t]\frac{d\bar{\Omega}}{d\rho}\hat{v}_r. \tag{133}$$

The problems (131)-(133) is subject to the boundary condition of least possible divergence for the axial velocity, and for the magnetized discs complemented by the vanishing conditions of the toroidal magnetic field at $\eta = \pm\infty$. As is indeed seen from that system, the magnetosonic wave is driven by the inertial wave, while the linear growth in time is entirely due to effect of the rotation shear, and disappears for $d\bar{\Omega}/d\rho = 0$.

As was mentioned above the two limits of small toroidal plasma beta as well as pure hydrodynamic system are considered analytically. If the scaled eigen-frequency of the inertia-coriolis waves (109), $\lambda = \pm 1$, do not coincide with the eigen-frequencies of the magnetosonic waves (118), $\lambda = \pm\sqrt{m+1}$, i.e. at $m \neq 0$, non-resonantly driven magnetosonic modes are excited. The stable magnetosonic modes may be excited resonantly by the inertial modes if any pair of respective eigen-values (109) with $\lambda = \pm 1$ and (118) with $\lambda = \pm\sqrt{m+1}$, coincide. It is easy to see that this may happen only for $m = 0$.

(i) Non-resonantly driven magnetosonic modes in the limit of small plasma beta. At vanishing plasma beta, β, in the leading order approximation Eq. (131) leads to a degenerate quasi-steady problem for $\hat{v}_z$ on the Keplerian time scale. Twice integrating Eq. (131) in η and setting arbitrary integration constants to zero, yield:

$$\hat{v}_z = \pm it\frac{d\bar{\Omega}}{d\rho}\int_0^\eta \hat{v}_r d\eta. \tag{134}$$

The rest unknown number density and toroidal magnetic field can be found at known $\hat{v}_z$ from non-degenerate unsteady relations (132) -(133).

(ii) Non-resonantly and resonantly driven magnetosonic modes in pure hydrodynamic discs. Setting $\bar{\beta}_\theta \equiv \infty$, $\hat{v}_r$ on the right-hand sides of (131) -(133) may be expanded in terms of the complete set of the spatial eigen-functions for the magnetosonic mode, namely, in the Hermite polynomials:

$$\hat{v}_r(\rho,\eta) = \sum_{m=0} W_{r,m}(\rho)H_m(\eta). \tag{135}$$

Examining the effect of a single term in the expansion above and utilizing the following recursion relation for the Hermite polynomials:

$$\frac{dH_m}{d\eta} = mH_{m-1}(\eta), \qquad m = 1,2,\ldots,$$

substituting the exponential anzatz (130) into Eq. (101), and keeping only terms that are proportional to t on its right hand side yield

$$\frac{1}{\bar{\Omega}^2}\frac{\partial^2 v_{z,m-1}}{\partial t^2} - \frac{\partial^2 v_{z,m-1}}{\partial\eta^2} + \eta\frac{\partial v_{z,m-1}}{\partial\eta} + v_{z,m-1} = \mp it\exp[\mp i\bar{\Omega}(\rho)t]\frac{d\bar{\Omega}}{d\rho}W_{r,m-1}(\rho)mH_{m-1}(\eta), \tag{136}$$

where for $m = 1$ the right hand side of Eq. (136) is a solution of the homogeneous part of the equation and hence represents a resonant driving force. For any other value of m the magnetosonic waves are driven non-resonantly. The typical non-resonant ($m = 2$) and resonant ($m = 1$) solution of Eq. (136) may be written in the following form:

$$v_{z,m-1} = \hat{v}_{z,m-1}(\rho,\eta,t)\exp[\mp i\bar{\Omega}(\rho)\theta] = \mp i\exp[\mp i\bar{\Omega}(\rho)t]W_{z,m-1}(\rho,t)H_{m-1}(\eta), \tag{137}$$

$$W_{z,1}(\rho,t) = (it\bar{\Omega})W^{(1)}_{z,1}(\rho) + W^{(0)}_{z,1}(\rho) \qquad \text{for} \quad m = 2, \tag{138}$$

$$W_{z,0}(\rho,t) = \frac{(it\bar{\Omega})^2}{2}W^{(2)}_{z,0}(\rho) + (it\bar{\Omega})W^{(1)}_{z,0}(\rho) \qquad \text{for} \quad m = 1. \tag{139}$$

Here the coefficients are determined through an arbitrary amplitude of the radial velocity $W_{r,1}(\rho)$ for non-resonant ($m = 2$) and resonant ($m = 1$) system, respectively, are as follows

$$\frac{W^{(1)}_{z,1}(\rho)}{W_{r,1}(\rho)} = -i\frac{2}{\bar{\Omega}}\frac{d\bar{\Omega})}{d\rho}, \quad \frac{W^{(0)}_{z,1}(\rho)}{W_{r,1}(\rho)} = \pm i\frac{2}{\bar{\Omega}}\frac{d\bar{\Omega}}{d\rho} \qquad \text{for} \quad m = 2, \tag{140}$$

$$\frac{W^{(2)}_{z,0}(\rho)}{W_{r,1}(\rho)} = \mp i\frac{1}{\bar{\Omega}}\frac{d\bar{\Omega})}{d\rho}, \quad \frac{W^{(1)}_{z,0}(\rho)}{W_{r,1}(\rho)} = -i\frac{1}{2}\frac{1}{\bar{\Omega}}\frac{d\bar{\Omega}}{d\rho} \qquad \text{for} \quad m = 1. \tag{141}$$

The corresponding expressions for number density and toroidal magnetic field may be derived from the rest equations of the system (132) -(133).

5 SUMMARY AND DISCUSSION

A comprehensive asymptotic analysis in small aspect ratio of the disc, ϵ, has been carried out of the response of thin vertically-isothermal Keplerian discs to small magnetohydrodynamic perturbations. Two regimes of axisymmetric instability have been identified depending on the type of equilibria in small aspect ratio of the disc, ϵ. The first is developed in the axially dominated equilibrium magnetic configurations, $\bar{B}_z \sim \epsilon^0$, and is excited at a relatively low level of hydrodynamic perturbations in the disc plane V_r', $V_\theta' \sim \epsilon^1$, while the second regime occurs in the toroidally dominated magnetic fields, $\bar{B}_\theta \sim \epsilon^0$, at relatively high level of hydrodynamic perturbations, V_r', $V_\theta' \sim \epsilon^0$ (the axial velocity perturbations are in both regimes of the same orders, $V_z' \sim \epsilon^1$, see Tables 1 and 2). As a result of that scaling, the pure hydrodynamic limit is achievable only within the second regime. Indeed, it is demonstrated that as distinct from the first regime, the second regime can not produce spectrally unstable modes, but excites a weak algebraic non-modal growth in time. The inertia-Coriolis driven magnetosonic mode leads to their non-resonant and resonant coupling that induces, respectively, the linear and quadratic in time growth of perturbations.

It should be emphasized though that that result is restricted to axisymmetric perturbations and nonaxisymmetric ones may give rise to spectral instabilities in the dominant toroidal field case as well as indeed is the case for magnetized Taylor-Couette flows (see Rudiger et al. 2007). Indeed, Terquem & Papaloizou (1996) have derived sufficient conditions for such instabilities in some sense of a thin disk limit. If such instabilities indeed exist they are of a transient nature as the radial wave number grows and drives the system out of the instability regime, Balbus & Hawley (1991). In addition, as demonstrated in Sections 3 and 4 spectrally unstable perturbations may occur if the Lorentz force is of the same order as the inertia terms. This means that the spectrally unstable non-axisymmetric perturbations are expected to be of higher order in ϵ than those considered in Section 4, that grow linearly and quadratically with time. Thus, it takes full nonlinear numerical calculations to determine which perturbations are more significant, namely, non-axisymmetric ones that grow exponentially from a very low level with a decreasing growth rate, or linearly and quadratically growing symmetric perturbations that grow from initial disturbances of much higher amplitudes.

For perturbations of type I the main accent is made on the dominant poloidal magnetic field, while the general case of comparable poloidal and toroidal components of the equilibrium magnetic field is discussed in Appendix A. Explicit solutions of the stability problem for the dominant equilibrium poloidal magnetic field of type I are obtained by replacing the true isothermal density vertical steady-state distribution $\bar{\nu}(\eta) = \exp(-\eta^2/2)$ by the hyperbolic function $\bar{\nu}(\eta) = \mathrm{sech}^2(b\eta)$ which has the similar shape and the same total mass of the disc. This model profile represents some true equilibrium that is obtained from a slightly different gravitational potential. The model eigenfunctions are exact solutions of the model very close to those obtained approximately by WKB from the true problem [Liverts & Mond (2009)], but they form the full family of explicit, simple and orthogonal eigenfunctions of the model problem. Such properties are significant for the consequent study of non-linear development of the instability.

A study of the stability of isothermal disks has been presented before in Gammie & Balbus (1994) and Latter et al. (2010), who have also utilized the model density profile $\mathrm{sech}^2\eta$. The main differences between those two works and the current investigation are:

(i) Gammie & Balbus (1994) and Latter et al. (2010) have approached the stability problem of the disk within the local setting of a shearing box described by local Cartesian coordinates. In contrast, in the current work the entire disk is considered and is described by the natural cylindrical coordinates with the aid of asymptotic analysis in the natural small parameter of the problem, namely, the ratio of the thickness of the disk to its characteristic radius $\sim \epsilon$.

(ii) Stemming from the shearing box local approach, the solutions for the perturbations that are given in Gammie & Balbus (1994) and Latter et al. (2010) are independent of the radial-like coordinate. In the current work, however, the radial derivatives drop out of the equations due to the asymptotic analysis in small ϵ. Consequently, the radial coordinate is a mere parameter in the subsequent calculations and conclusions. Thus, the result is that perturbations are excited on each separate cylindrical shell, independently of the other shells, with amplitude that depends arbitrarily on the radius through some initial conditions. As a result, it comes out rigorously that the stability conditions depend on the radius, and different rings within the disk have different stability properties, like number of unstable modes as well as growth rates.

(iii) The current work includes also analysis of the acoustic spectrum. Though stable in the case of purely axial magnetic field (explicit expressions are derived for the eigenvalues as well as for the eigenfunctions), as is sketched in Appendix A for large plasma beta, a toroidal component of the same order of magnitude as the axial one leads to the driving of acoustic modes by unstable MRI's.

(iv) Figure 1 demonstrates that best choice of the parameter b is obtained from the requirement of identical total mass of the disc for the two density profiles, $\bar{\nu}(\eta) = \exp(-\eta^2/2)$ and $\bar{\nu}(\eta) = \mathrm{sech}^2(b\eta)$.

In addition a qualitative analysis of the influence of the equilibrium toroidal magnetic field of type I on the disc stability

is carried out in Appendix A in the limit of large plasma beta on two characteristic scales of AC's and MS's modes. In that case as distinct from the small plasma beta ($\beta \lesssim 1$), the AC and MS modes are decoupled. On the characteristic scale of AC's mode, this leaves the resulting dispersion relation the same as in the case of the dominant poloidal magnetic field (zero toroidal magnetic field), and the influence of the toroidal magnetic field is reduced to excitation of the AC-driven MS mode. On the characteristic scale of MS's mode, a stable MS mode decouples from the AC mode and the influence of the toroidal magnetic field is reduced to excitation of the stable MS-driven AC mode.

In the present work the model of the non-modal instability [Shtemler et al. (2010)] for pure hydrodynamic adiabatic discs is adopted for more realistic vertically-isothermal discs with diffused density vanishing at infinity. The model is also extended on magnetized discs with type II equilibria. Within that model the eigenvalue problem has been solved in the characteristic cases of small and large plasma beta as well as for pure hydrodynamic systems. Furthermore, the magnetosonic waves driven non-resonantly with inertia-Coriolis ones are considered in the limit of small toroidal plasma beta, as a typical example. Since in the limits of large and small plasma beta, the magnetosonic modes are excited with high scaled frequency, $\lambda \gg 1$, they can not be resonantly driven by the low-frequency inertial-Coriolis mode with $\lambda \pm 1$. By this reason the resonantly driven magnetosonic modes are calculated for only the pure hydrodynamic system, in order to illustrate a quadratic in time growth of perturbations. The rotation shear is found to be responsible for the linear and quadratic growth in time. Furthermore, compressible inertia-coriolis stable oscillations continuously pump energy from the sheared steady state equilibrium and transfer it (resonantly as well as non resonantly) to the continuously algebraically growing magnetosonic waves. Compressibility is indeed inevitable due to the supersonic rotation of the steady-state disc combined with its small vertical dimensions which make the vertical magnetosonic crossing time of the order of a rotation period. As distinct from MRI the non modal growth is exhibited for all admissible parameters of the system.

Note that the present study has been restricted by consideration of the axisymmetric perturbations only. In particular, for type II perturbations the adopted analysis is considered as the necessary step in achieving a complete picture of transition to turbulence in accretion discs. First, it provides the instability for the case of very weak magnetic fields close to pure hydrodynamic perturbations in the discs. Furthermore, since the magnetized discs are stable with respect to axisymmetric normal modes, an alternative scenario of an algebraic instability has been investigated. The present analysis of both resonantly and non-resonantly driven magnetosonic modes is interesting in the context of the well known scenario for sub-critical transition to turbulence Schmidt & Henningson (2001), since the non-spectral mechanism of the power growth in time provides instability even for the system parameters of the discs stable with respect to normal modes. The considered scenario leaves to be valid for sub-critical parameters of the discs within more general model of non-axisymmetric MRI [e.g. Balbus & Hawley (1991), Terquem & Papaloizou (1996), Foglizzo & Tagger (1995)].

APPENDIX A: STABILITY FOR COMPARABLE IN-PLANE EQUILIBRIUM MAGNETIC FIELDS

The general relations for comparable in-plane components of the equilibrium magnetic field of type I are presented below. Substituting the exponential anzatz (42)-(43) into the general system (36)-(41) results in the following system of linear ordinary differential equations (parametrically depending on the radial variable r) for the perturbed toroidal magnetic field and axial velocity, $\hat{b}_\theta$ and $\hat{v}_z$:

$$L_{AC}\hat{b}_\theta = \frac{1}{2}\bar{S}(r)\bar{\beta}_z(r)\Big\{\frac{d}{d\eta}\left[\frac{1}{\bar{\nu}(\eta)}\frac{d^2\hat{v}_z}{d\eta^2}\right] - 3(\lambda^2-1)\bar{\beta}_z(r)\frac{d\hat{v}_z}{d\eta}\Big\}, \tag{A1}$$

$$L_{MS}\hat{v}_z = -i\lambda\frac{\bar{S}(r)}{\bar{\beta}_z(r)}\frac{d}{d\eta}\left[\frac{\hat{b}_\theta}{\bar{\nu}(\eta)}\right]. \tag{A2}$$

Here $\bar{S}(r)$ is the coupling coefficient between AC and MS modes,

$$L_{AC}\hat{b}_\theta \equiv \frac{d}{d\eta}\Big\{\frac{1}{\bar{\nu}(\eta)}\frac{d^2}{d\eta^2}\left[\frac{1}{\bar{\nu}(\eta)}\frac{d\hat{b}_\theta}{d\eta}\right]\Big\} + (3+2\lambda^2)\bar{\beta}_z(r)\frac{d}{d\eta}\left[\frac{1}{\bar{\nu}(\eta)}\frac{d\hat{b}_\theta}{d\eta}\right] + \lambda^2(\lambda^2-1)\bar{\beta}_z^2(r)\hat{b}_\theta, \tag{A3}$$

$$L_{MS}\hat{v}_z \equiv \frac{d^2\hat{v}_z}{d\eta^2} + \frac{1}{\bar{\nu}(\eta)}\frac{d\bar{\nu}(\eta)}{d\eta}\frac{d\hat{v}_z}{d\eta} + \Big\{\lambda^2 + \frac{d}{d\eta}\Big[\frac{1}{\bar{\nu}(\eta)}\frac{d\bar{\nu}(\eta)}{d\eta}\Big]\Big\}\hat{v}_z \equiv \frac{d^2\hat{v}_z}{d\eta^2} - \eta\frac{d\hat{v}_z}{d\eta} + (\lambda^2-1)\hat{v}_z. \tag{A4}$$

Equations (A1) - (A2) are complemented by the boundary conditions of the toroidal magnetic field vanishing and of the least possible divergence for the axial velocity at infinity. The operators L_{AC} and L_{MS} are such that the two principal, AC and MS, modes satisfy the following homogeneous problems for zero equilibrium toroidal magnetic field (i.e. for zero coupling coefficient $\bar{S}(r) \equiv 0$) with the same boundary conditions:

$$L_{AC}\hat{b}_\theta = 0, \tag{A5}$$

$$L_{MS}\hat{v}_z = 0. \tag{A6}$$

Below that problem will be considered for large plasma beta on two characteristic scales of AC's and MS's modes.

A1 Zero toroidal magnetic field.

First consider the problem for zero coupling coefficient, $\bar{S}(r)$. Note that if set $\bar{S}(r) = 0$, the equilibrium toroidal magnetic field has no input in the thin disc approximation under consideration, the problems for AC and MS modes are decoupled, and can be considered separately (as in Section 3 above). The method of two-scale asymptotic expansions in large plasma-beta will be applied below, which is convenient for the qualitative analysis of the disc stability. The method is equivalent to WKB approach to the problem (A5) for MRI mode that also implicitly assumes $\beta >> 1$. In that connection note that as is demonstrated in Liverts & Mond (2009) the WKB approximation for MRI mode well describes the exact numerical solution up to plasma beta $\beta \sim 1$ (see also Section 3 where the WKB approximation is mentioned very close to the exact explicit solution for model density profile).

According to the method of two-scale asymptotic expansions [see e.g. Nayfeh (1973)], let us introduce the slow, $\bar{\eta}$, and fast, $\tilde{\eta}$, variables at $\beta >> 1$ for AC mode:

$$\bar{\eta} = \eta, \;\; \tilde{\eta} = \beta^a \int_0^\eta g(\eta)\eta, \quad (a > 0), \;\; \tilde{\beta}_z(r) = \frac{\bar{\beta}_z(r)}{\beta} \sim \beta^0, \;\; \frac{d}{d\eta} = \beta^a \Big[g(\bar{\eta}) \frac{\partial}{\partial \tilde{\eta}} + \beta^{-a} \frac{\partial}{\partial \bar{\eta}} \Big], \tag{A7}$$

$$\hat{b}_\theta(\eta) = \hat{b}_{\theta,0}(\bar{\eta}, \tilde{\eta}) + \beta^{-a} \hat{b}_{\theta,1}(\bar{\eta}, \tilde{\eta}) + \ldots, \;\; \lambda = \lambda_0 + \beta^{-a}\lambda_1 + \ldots. \tag{A8}$$

Applying the principle of the least possible degeneration of the problem yields:

$$a = 1/2. \tag{A9}$$

To make the coefficients of the leading order equation (A1) independent of the slow variable, set

$$g(\bar{\eta}) = \bar{\nu}^{1/2}(\bar{\eta}). \tag{A10}$$

This yields

$$\frac{\partial^4 \hat{b}_{\theta,0}}{\partial \tilde{\eta}^4} + (3 + 2\lambda_0^2)\tilde{\beta}_z(r) \frac{\partial^2 \hat{b}_{\theta,0}}{\partial \tilde{\eta}^2} + \lambda_0^2(\lambda_0^2 - 1)\tilde{\beta}_z^2(r)\hat{b}_{\theta,0} = 0. \tag{A11}$$

The vanishing at infinity solution of the linear equation (A11) can be easily found explicitly to leading order in β up to amplitude factors that depend on slow variable, $\bar{\eta}$. The equation (A11) evidently conserves all the principle derivatives by fast variable in the exact Eq. (A5). The dependence of the amplitude factors on the slow variable are determined by the problem of the next order approximation in large plasma beta. To leading order in β, these two first leading order problems completed by the corresponding boundary conditions fully determine the approximate solution of the problem including the dispersion relation for the eigenvalue λ_0.

A2 Comparable toroidal and poloidal magnetic fields at the characteristic scale of AC mode.

Let us now apply the two-scale asymptotic expansions (A7) - (A8) in $\beta >> 1$ to complete relations (A1) - (A4) for the mixed toroidal and poloidal magnetic fields on the characteristic scale of AC's mode. It is assumed as above in the case of separated AC mode that $a > 0$, and additionally

$$\bar{S}(r) = \sqrt{\frac{\bar{\beta}_z(r)}{\bar{\beta}_\theta(r)}} \sim \beta^0, \;\; \hat{v}_z(\eta) = \beta^c f(\bar{\eta})[\hat{v}_{z,0}(\bar{\eta}, \tilde{\eta}) + \beta^{-a}\hat{v}_{z,1}(\bar{\eta}, \tilde{\eta}) + \ldots], \;\; \lambda = \lambda_0 + \beta^{-1}\lambda_1 + \ldots. \tag{A12}$$

(i) *Leading order approximation.* The principle of the least possible degeneration of the problem yields:

$$a = 1/2, \;\; c = -2. \tag{A13}$$

To make the coefficients of the resulting relations to leading order independent of the slow variable, set

$$g(\bar{\eta}) = \bar{\nu}^{1/2}(\bar{\eta}), \;\; f(\bar{\eta}) = \bar{\nu}^{-3/2}(\bar{\eta}). \tag{A14}$$

This leaves Eq. (11) valid for the AC mode

$$\frac{\partial^4 \hat{b}_{\theta,0}}{\partial \tilde{\eta}^4} + (3 + 2\lambda_0^2)\tilde{\beta}_z(r) \frac{\partial^2 \hat{b}_{\theta,0}}{\partial \tilde{\eta}^2} + \lambda_0^2(\lambda_0^2 - 1)\tilde{\beta}_z^2(r)\hat{b}_{\theta,0} = 0, \tag{A15}$$

while the MS mode is the AC-driven mode

$$\frac{\partial \hat{v}_{z,0}}{\partial \tilde{\eta}} = -i\lambda_0 \frac{\bar{S}(r)}{\tilde{\beta}_z(r)} \hat{b}_{\theta,0}. \tag{A16}$$

Thus, in the limit of large plasma beta, the AC mode decouples on its characteristic scale from the MS mode, and the influence of the toroidal magnetic field leaves the problem for the AC mode the same as in the case of zero equilibrium toroidal field, and simultaneously induces the AC-driven MS mode.

(ii) *On the next order approximations.* Note that the leading-order governing relation for $\hat{b}_{\theta,0}$ is of the order of β^2, while the next-order relation for $\hat{b}_{\theta,1}$ is of the order of $\beta^{3/2}$. Estimating the terms, which are proportional to the coupling coefficient $\bar{S}(r)$ and induced by the equilibrium toroidal magnetic field, note that they are of the order of $\beta^{1/2}$, i.e. much less than $\beta^{3/2}$. Hence the toroidal magnetic field has no input neither to the leading- nor to the next-order approximations, which determine the resulting approximate solution of the problem. In particular, this leaves the resulting dispersion relation the same as in the case of zero equilibrium toroidal magnetic field considered in Section 3.

A3 Comparable toroidal and poloidal magnetic fields at the characteristic scale of MS mode.

In that case the conventional asymptotical method of subsequent interactions may be applyied:

$$\bar{S}(r)=\sqrt{\frac{\bar{\beta}_z(r)}{\bar{\beta}_\theta(r)}}\sim\beta^0,\ \ \tilde{\beta}_z(r)=\frac{\bar{\beta}_z(r)}{\beta}\sim\beta^0, \tag{A17}$$

$$\hat{b}_\theta(\eta)=\hat{b}_{\theta,0}(\eta)+\beta^{-1}\hat{b}_{\theta,1}(\eta)+\ldots,\ \ \hat{v}_z(\eta)=\hat{v}_{z,0}(\eta)+\beta^{-1}\hat{v}_{z,1}(\eta)+\ldots,\ \ \lambda=\lambda_0+\beta^{-1}\lambda_1+\ldots. \tag{A18}$$

Substituting (A17)-(A18) in (A1) - (A4), and applying the principle of the least possible degeneration of the problem yield that the equation for $\hat{v}_{z,0}$ and $\hat{b}_{\theta,0}(\eta)$ are reduced to the conventional relation (A6) for MS mode with the eigenvalues $\lambda_0=\sqrt{m+1}$, ($m=1,2,\ldots$, see Eq. (71))

$$\frac{d^2\hat{v}_{z,0}}{d\eta^2}-\eta\frac{d\hat{v}_{z,0}}{d\eta}+(\lambda_0^2-1)\hat{v}_{z,0}=0, \tag{A19}$$

and to the relation for the MS-driven AC mode

$$\hat{b}_{\theta,0}=-\frac{3}{2\lambda_0^2}\bar{S}(r)\frac{d\hat{v}_{z,0}}{d\eta}. \tag{A20}$$

Thus, on the characteristic scale of MS's mode, the stable MS mode decouples from the AC mode at large plasma beta, and the influence of the toroidal magnetic field is reduced to excitation of the stable MS-driven AC mode.

Finally note that above qualitative asymptotic analysis of the problem in the limit of large plasma beta demonstrates both spectral and transient stability of the disc embedded in the mixed equilibrium toroidal and poloidal magnetic fields of comparable values.

REFERENCES

Balbus S. A., & Hawley J. F., 1991, ApJ, **376**, 214
Balbus S. A., & Hawley J. F., 1992, ApJ, **400**, 610
Begelman M.C. & Pringle J.E., 2007, MNRAS, **375**, 1070
Bodo G., Mignone A., Cattaneo F., Rossi P., and Ferrari A., A&A, **487**, 1
Brandenburg A., Nordland A., Stein R. F., Torkelson U., 1995, ApJ, **446**, 741
Chandrasechar S., 1960, Proc. Natl. Acad. Sci. A, **46**, 46, 223
Coppi B., & Keyes E.A., 2003, ApJ, **595**, 1000
Foglizzo T., and Tagger M., 1995, A&A, **301**, 293
Frank J., King A., and Raine D., 2002, *Acreation Power in Astrophysics* , (Cambridge: University Press).
Fromang S., and Papaloizou J., 2007, A&A, **476**, 1113
Fromang S., Papaloizou J., Lesur G., Heineman T., 2007, A&A, **476**, 1123
Gammie C. F., & Balbus S. A., 1994, MNRAS, **270**, 138
Hawley J. F., Gammie C. F., Balbus S. A., 1996, ApJ, **464**, 690
Hawley J. F., & Krolik J. H., 2002, ApJ, **566**, 164
Landau L. D. and Lifshits E. M., 1977, *Quantum mechanics, Non-Relativistic Theory* , (N.-Y.: Pergamon Press).
Latter H. N., Fromang S., Gressel O., 2010 MNRAS, **406**, 848
Lesur G., and Longaretti P. Y., 2007, MNRAS, **378**, 1471
Liverts E. and Mond M., 2009, MNRAS, **392**, 287
Migdal A. B., 1977, *Qualitative Methods in Quantum Physics*, (Massachusetts: W. A. Bnejamin Inc.).
Nayfeh A. H., 1973, *Perturbation Methods*, (New-York: John Willey & Sons).
Papaloizou J. C. B., & Terquem C., 1997, MNRAS, **287**, 771

Pessah M.E. and Psaltis D., 2005, ApJ, **628**, 829
Pessah M. E., Chan C. K., Psaltis D., 2007, ApJ, **668**, L51
Proga D., 2003, ApJ, **585** 406
Rebusco P., Umurhan O. M., Kluzniak W., and Regev O., 2009, Phys. Fluids, **21**, 076601
Regev O., and Umurhan O. M., 2008, A&A, **481**, 21
Rudiger G., Hollerbach R., Schultz M., and Detlev E., 2007, MNRAS, **377**, 1481
Schmidt P. J., and Henningson D. S., 2001, *Stability and transition in Shear Flows* , (Berlin: Springer).
Shtemler Y. M., Mond M., & Rudiger G., 2009, MNRAS, **394**, 1379
Shtemler Y. M., Mond M., Rudiger G, Regev O., & Umurhan O.M., 2010, MNRAS, **406**, 517
Spitzer L., 1942, ApJ, **95**, 329
Terquem C., & Papaloizou J. C. B., 1996, MNRAS, **279**, 767
Velichov E. P., 1959, Zh. Eksp. Teor. Fiz., **36**, 1398 [English translation, 1959, Sov. Phys. JETP, 36, 95]
Umurhan O. M., Nemirovsky A., Regev O., & Shaviv G., 2006, A&A, **446**, 1

This paper has been typeset from a TEX/ LATEX file prepared by the author.